Along-dip variations of subduction fluids: The 30–80 km depth traverse of the Schistes Lustrés complex (Queyras-Monviso, W. Alps)

Clément Herviou, Anne Verlaguet, Philippe Agard, Michele Locatelli, Hugues Raimbourg, Benjamin Lefeuvre, Benoît Dubacq

Journal Pre-proof

Along-dip variations of subduction fluids: The 30–80 km depth traverse of the Schistes Lustrés complex (Queyras-Monviso, W. Alps)

Clément Herviou, Anne Verlaguet, Philippe Agard, Michele Locatelli, Hugues Raimbourg, Benjamin Lefeuvre, Benoit Dubacq
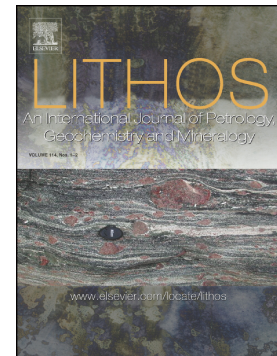
Please cite this article as: C. Herviou, A. Verlaguet, P. Agard, et al., Along-dip variations of subduction fluids: The 30–80 km depth traverse of the Schistes Lustrés complex (Queyras-Monviso, W. Alps), *LITHOS* (2021), https://doi.org/10.1016/j.lithos.2021.106168

This is a PDF file of an article that has undergone enhancements after acceptance, such as the addition of a cover page and metadata, and formatting for readability, but it is not yet the definitive version of record. This version will undergo additional copyediting, typesetting and review before it is published in its final form, but we are providing this version to give early visibility of the article. Please note that, during the production process, errors may be discovered which could affect the content, and all legal disclaimers that apply to the journal pertain.

Along-dip variations of subduction fluids: the 30-80 km depth traverse of the Schistes Lustrés complex (Queyras-Monviso, W. Alps)

Clément Herviou[a,][*] clement.herviou@sorbonne-universite.fr, Anne Verlaguet[a], Philippe Agard[a], Michele Locatelli[b], Hugues Raimbourg[c], Benjamin Lefeuvre[a], Benoit Dubacq[a]

[a]Sorbonne Université, CNRS-INSU, Institut des Sciences de la Terre de Paris, ISTeP UMR 7193, F 75005 Paris, France

[b]Dipartimento di Scienze della Terra, Ambiente e Vita (DISTAV), Università di Genova, Italy

[c]Institut des Sciences de la Terre d'Orléans (ISTO), UMR7327 Université d'Orléans, CNRS-INSU, Bureau de Recherches Géologiques et Minières (BRGM), 45071 Orléans, France

[*]Corresponding author.

Abstract

The Queyras-Monviso traverse of the Schistes Lustrés complex, is a stack of underplated nappes of oceanic rocks subducted from blueschist- to eclogite-facies conditions.

This study reports on salinities and gas contents of primary fluid inclusions trapped in high pressure veins from metasediments and metamafic rocks (445 fluid inclusions in 22 samples). These data provide snapshots of the compositions of fluids present at peak burial conditions, varying from ~30 to 80 km depth and illustrate the evolution of fluid composition with burial along a cold subduction zone.

Fluid inclusions trapped in lawsonite- and carpholite-bearing veins in metasediments contain moderately saline aqueous fluids (average salinity of 4.6 wt% NaCl eq.) with subordinate amounts of CO_2 and CH_4 in the vapor phase. The observed salinity decrease with increasing grade is interpreted as reflecting progressive dilution of initial seawater-like pore fluid by low-salinity fluids released locally by dehydration reactions. Less-frequently measured higher salinities in the uppermost metasedimentary-dominated tectonic unit suggest brine infiltration from embedded blocks of margin units containing evaporites. CO_2 and CH_4 (and scarce potential hydrocarbons) appear to be locally released from fluid interaction with carbonates and carbonaceous matter-rich pelitic horizons, respectively.

Fluid inclusions in high pressure omphacite veins in metagabbros record higher salinities (mean salinity about 17 wt% NaCl eq.) with small amounts of N_2 in eclogitic veins only, and a variety of minerals (calcite, white mica, salts) indicative of complex chemical systems. These high salinities are interpreted as partly inherited from seafloor high-temperature hydrothermal alteration of gabbros, resulting in phase separation and brine formation. Progressive breakdown of hydrothermal Cl-rich amphibole to glaucophane (blueschist-facies) and then omphacite (eclogite-facies) and release of brines trapped in fluid inclusions could account for

the high salinity fluids. Therefore, in metagabbros, fluid inclusions record progressive release of Cl in the fluid phase with increasing grade.

Fluid signatures of metasediments and metamafics appear characteristic of each rock type. Local fluid signatures and redox conditions were preserved within units, possibly due to restricted and transient fluid circulation (at the hm-scale at most).

Fluid inclusions in Alpine metasediments show salinities and gas contents comparable with other subducted fragments of oceanic lithosphere worldwide, whereas fluid salinities of Alpine metagabbros are higher than salinities recorded elsewhere, either due to (1) higher-temperature hydrothermal alteration and brine formation in Alpine metagabbros (compared to metavolcanics) or (2) more restricted infiltration by sediment-derived fluids compared to block-in-mélange subduction complexes.

Keywords: Fluid inclusions; Subduction fluids; Schistes Lustrés; Western Alps; Fluid-rock interactions; Salinity variations

1. Introduction

Large amounts of fluids are released in subduction zones by progressive dehydration of hydrothermalized portions of the oceanic lithosphere and of its sedimentary cover (Rüpke et al., 2004; Hacker, 2008; Schmidt and Poli, 2014). Fluid release and fluid migration have major mechanical and chemical consequences in rocks: the presence of a free fluid phase strongly impacts rheology, e.g. fracturing and intermediate-depth earthquake and slow slip event generation (Obara, 2002; Hacker et al., 2003; Hyndman et al., 2015); the amount and composition of fluids, in part controlled by permeability, dictates the magnitude of chemical changes and mass transfer. Characterizing major fluid sources, amounts and pathways in subduction zones is therefore a prerequisite to assessing their impact on subduction dynamics (Bebout and Penniston-Dorland, 2016).

Fluids are elusive in essence and their compositions are mostly inferred from isotopic and trace element studies from exhumed fossil subduction zones (Spandler and Pirard, 2013). A direct access to deep fluid compositions is nevertheless provided by primary fluid inclusions (FI) trapped in high pressure low temperature (HP-LT) minerals (e.g., Scambelluri and Philippot, 2001; Touret and Frezzotti, 2003; Frezzotti and Ferrando, 2015). Despite common re-equilibration of FI densities during exhumation and difficulty to preserve V-X properties of FI trapped at prograde or peak metamorphic conditions (Vityk and Bodnar, 1995a, 1995b; Küster and Stöckhert, 1997; Bodnar, 2003b; Diamond, 2003; Tarantola et al., 2012; Raimbourg et al., 2018), several studies have shown that their pristine compositions may be genuinely preserved (Sterner and Bodnar, 1989; Diamond et al., 2010; Diamond and Tarantola, 2015).

Former studies of subduction FI have so far mostly focused on shallow metasediments from exhumed accretionary wedges (e.g., Brantley et al., 1998; Smith and Yardley, 1999; Raimbourg et al., 2015) or mafic and ultramafic rocks from deep eclogitic metamorphic terranes (e.g., Philippot and Selverstone, 1991; Giaramita and Sorensen, 1994; Fig. 1; Table 1). As shown by the compilation of figure 1, only few studies have provided information on fluid compositions in blueschist-facies metapelites (Agard et al., 2000; El-Shazly and Sisson, 2004) despite their (i) considerable fluid content stored in hydrous minerals (e.g., Bousquet et al. 2008; Lefeuvre et al., 2020) and (ii) potential to retain some elements to great depths (Busigny et al., 2003; Bebout et al., 2013), and thereby contribute to a significant fraction of fluids released at depth and element recycling. Moreover, the evolution of fluid compositions with increasing P-T conditions remains poorly documented in both sedimentary and mafic protoliths and somewhat ambiguous. Local dehydration and progressive dilution of pore water has been proposed to explain the decrease of fluid salinity in prehnite-pumpellyite- to blueschist-facies Franciscan metasediments (Sadofsky and Bebout, 2004), whereas preservation of hydrothermal salinities up to eclogite facies conditions has been proposed for Alpine mafic rocks (e.g., Philippot et al., 1998). To assess wether such trends are representative across subduction zones, there is a need for statistical data on the evolution of fluid composition with depth in both mafic rocks and sediments, i.e. on a continuous transect of a single subduction zone.

In the Western Alps, several tectonic slices buried from ~30 km to ~80 km during subduction of the Liguro-Piemont ocean are continuously exposed in the Schistes Lustrés complex (SL; Agard et al., 2001, 2009). They comprise oceanic metasediments with variable mafic and ultramafic fragments and have preserved prograde to peak metamorphic assemblages and abundant veins with HP minerals (Goffé and Chopin, 1986; Philippot, 1987; Lefeuvre et al., 2020). They provide the opportunity to study the evolution of fluid compositions and pathways across depths along a former subduction plate interface (Agard et al., 2018). Isotopic and trace element data of this dominantly metasedimentary suite suggest the dominance of a rock-buffered system with only limited external fluid infiltration (Henry et al., 1996; Busigny et al., 2003; Bebout et al., 2013; Cook-Kollars et al., 2014), except along major tectonic contacts (Spandler et al., 2011; Angiboust et al., 2011, 2014; Locatelli et al., 2018; Jaeckel et al., 2018; Epstein et al., 2021). The current dataset of primary FI of HP veins shows aqueous low to moderately saline fluid compositions in the shallowest SL (Agard et al., 2000; locally CO_2-bearing: Raimbourg et al., 2018) and moderate to highly-saline fluids in the deep mafic and ultramafic eclogite-facies rocks (Philippot and Selverstone, 1991; Nadeau et al., 1993; Scambelluri et al., 1997; Philippot et al., 1998).

The aim of the present study is to characterize the composition of fluids trapped in FI from HP veins formed at or close to peak burial, across subduction depths and for two major fluid-reservoirs/sources, i.e. metasediments and metamafic rocks. To obtain a statistically meaningful dataset representative of the evolution of fluid composition with burial, we report analyses of 445 FI in 22 samples collected along the Queyras-Monviso transect of the Alpine subduction zone. We then discuss possible fluid sources, evaluate the relative contributions of inherited sedimentary and/or hydrothermal fluids and of local devolatilization reactions and/or external deeper fluids, and finally discuss implications for fluid-rock interactions and evolution of fluid composition along the subduction plate interface.

2. Geological setting

2.1. Fragments of subducted oceanic lithosphere in the Western Alps

The Western Alps formed as a result of an east- to south-east-dipping and slow (~1 cm/yr) subduction of the ~700 km wide Valais and Liguro-Piemont oceans below Adria/Apulia (Le Pichon et al., 1988; Schmid et al., 1996, 2017; Rpen et al., 2003; Handy et al., 2010; Agard and Handy, 2021). Subduction of these slow-spreading oceanic domains (Lagabrielle and Cannat, 1990) started in the late Cretaceous and was over by ~35 Ma (Stampfli et al., 1998; Schmid et al., 2017).

Remants of subducted Liguro-Piemont oceanic lithosphere are now exposed in the internal domain of the Western Alps and form a nappe stack known as the Schistes Lustrés complex (SL; Agard et al., 2009; Agard, 2021). Metasediments are volumetrically dominant in this complex and range from late Jurassic (De Wever and Caby, 1981; Lagabrielle, 1987) to late Cretaceous (Lemoine et al., 1984; Lagabrielle, 1987). They correspond to an initial ~200-400 m thick sequence of pelagic seafloor deposits (marls, shales and limestones metamorphosed as calcschists, pelites and marbles; Lemoine et al., 1984; Lemoine and Tricart, 1986; Deville et al., 1992; Michard et al., 1996) now embedding variable amounts of mafic and ultramafic rocks. During subduction, these metasediments were buried to contrasting depths and were intensely folded, leading to a consequent thickening of the initial sedimentary pile (Agard et al., 2002; Tricart and Schwartz, 2006). Agard et al. (2009) have roughly estimated that approximatively 30% to 50% of the sedimentary deposits were offscraped from the downgoing subducting plate and exhumed, whereas only ~5% of the oceanic crust and serpentinized mantle did.

2.2. Tectono-metamorphic evolution of the Schistes Lustrés complex

Based on lithostratigraphic and tectono-metamorphic contrasts, several units were identified in the SL complex (Lagabrielle, 1987; Agard et al., 2009). A major distinction is between the blueschist- (BS) facies metasedimentary-dominated units and the metamafic-ultramafic-dominant eclogite-facies units cropping out eastward of and tectonically below the BS-facies units (Fig. 2a; Dal Piaz, 1974; Caby et al., 1978; Droop et al., 1990; Pognante, 1991). These groups of units are separated by a major extensional tectonic contact (Philippot, 1990; Ballèvre et al., 1990; Ballèvre and Merle, 1993). Three distinct groups, from west to east, can be recognized in the SL complex (Fudral et al., 1987; Fudral, 1996; Lagabrielle et al., 2015; Plunder et al., 2012; Agard, 2021): (1) the upper units (LPU) exposed on the westernmost part of the SL complex are mostly made of low- to medium-temperature BS-facies calcschists and pelites with minor mafic-ultramafic fragments; (2) the middle units (LPM) comprise medium- to high-temperature BS-facies calcschists generally more carbonate-rich, with more oceanic slivers than the LPU; (3) the lower units (LPL) comprise transitional BS-eclogite-facies to eclogite-facies km-scale bodies of mafic and ultramafic rocks together with minor amounts of metasediments. In places, a distinction (not made in the following, for the sake of clarity) can be made between metasedimentary-rich tectonic slices (e.g., around Susa; Agard et al., 2001; Ghignone et al., 2020) and mafic/ultramafic units several km-long (e.g., Monviso; Lombardo, 1978; Locatelli et al., 2019a). The latter directly overly the internal crystalline massifs in the easternmost part of the SL complex.

P-T estimates show an eastward, almost continuous increase in metamorphic grade from the upper (1.2 GPa-300 °C) to the lower units (~2.5 GPa-550 °C), along a ~8 °C/km metamorphic gradient (Agard et al., 2001; Beyssac et al., 2002; Gabalda et al., 2009; Plunder et al., 2012; Schwartz et al., 2013).

Several deformation stages were identified and dated in the SL complex of the Cottian Alps (Agard et al., 2001, 2002; see also Ghignone et al., 2020): the first episode (D1) relates to the development of early fabrics, km-scale folds and crystallization of peak metamorphic assemblages at ~62-55 Ma. A second phase (D2) at ~51-45 Ma corresponds to the ductile east-vergent deformation accompanying early exhumation under BS-facies conditions. The third fabric (D3), between ~38 and 35 Ma, is marked by top-to-the-west ductile to brittle deformation associated with greenschist-facies exhumation, and coincides with the final ductile exhumation of large mafic-ultramafic complexes such as Monviso (Angiboust and Glodny, 2020). Two late fabrics (D4 and D5; Tricart and Schwartz, 2006), marked by small-scale boudinage and west-dipping normal faulting, characterize the final ductile-brittle transition during late exhumation.

2.3. The Queyras-Monviso traverse

This study focuses on the southern SL complex where subducted oceanic fragments buried at different depths are particularly well-exposed along the Queyras-Monviso traverse and provide access to fluid-rock interactions during subduction. In this area, four major units were identified (Figs. 2b, c; Lagabrielle, 1987; Lagabrielle et al., 2015).

Peak burial conditions across the traverse were constrained by mineralogical assemblages of meta-ophiolitic bodies (e.g., Schwartz, 2000; Tricart and Schwartz, 2006; Angiboust et al., 2012b; Locatelli et al., 2018) and maximum temperatures derived from the Raman spectroscopy of carbonaceous material (Angiboust et al., 2012b; Schwartz et al., 2013). From west to east, the two first units comprise metasedimentary-dominated low- to medium-temperature blueschists, while the third one was buried up to medium- to high-temperature BS-facies conditions. Lithologies and P-T conditions suggest that these slices are similar to the LPU and LPM cropping out further north in the Cottian Alps and Savoy (Agard et al., 2001; Plunder et al., 2012; Agard, 2021), and will be referred to below as LPU1, LPU2 and LPM (Figs. 2b, c; 3).The last unit on this traverse corresponds to the Monviso massif, a large mafic-ultramafic body comprising at least two sub-units metamorphosed at the BS- eclogite-facies transition and lawsonite-bearing eclogite facies (Schwartz et al., 2000; Angiboust et al., 2012b; Locatelli et al., 2018; Fig. 3), which can be regarded as an analogue to the LPL of the Cottian Alps, Savoy and Aosta-Valais (Deville et al., 1992; Agard et al., 2001; Angiboust et al., 2009; Plunder et al., 2012; Agard, 2021).

After peak burial between 62 and 55 Ma for LPU and LPM (Agard et al., 2002) and around 50-45 Ma for the Monviso LPL (Rubatto and Hermann, 2003; Rubatto and Angiboust, 2015; Garber et al., 2020), the four units of the Queyras-Monviso transect were exhumed from late Eocene to Miocene times (Schwartz et al., 2007, 2020; Angiboust and Glodny, 2020)

3. High pressure metamorphic veins

3.1. HP veins in the Schistes Lustrés complex

Metamorphic veins, as well as mineralized fractures and shear zones, provide access to fluid-rock interactions and fluid circulation pathways. BS-facies metasediments of the SL complex contain numerous veins (Fig. 4a), as for most former subduction complexes of various grades (Fisher and Byrne, 1990; Vannucchi, 2001; Sadofsky and Bebout, 2004; Meneghini et al., 2009; Raimbourg et al., 2015; Muñoz-Montecinos et al., 2020). Cartwright and Buick (2000) estimated that veins can make up to 30% of outcrops and commonly 5-10% of BS-facies metasediments in Alpine Corsica. Late veins, not studied here, are filled by

quartz ± calcite ± albite ± chlorite assemblages and relate to D2 and D3 exhumation events (Agard et al., 2000).

In metasediments, veins formed during (peak) burial are quartz-bearing and characterized by HP minerals such as lawsonite and Fe-Mg carpholite (Figs. 4a-f). These hydrous minerals, which contain 12 wt% H_2O, are abundant in the SL complex (Caron, 1974; Goffé and Chopin, 1986; Sicard-Lochon, 1987), with lawsonite and lawsonite pseudomorphs making up to 40-45 vol% of the host-rock in places (Lefeuvre et al., 2020).

Fe-Mg carpholite in the schist is commonly replaced by chlorite and white mica during exhumation and only preserved as micrometric needles inside quartz crystals (Goffé and Chopin, 1986; Agard et al., 2000, 2001) or in meter-scale quartz-pods/veins subparallel to the main D1/D2 foliation (Agard et al., 2000).

Lawsonite is less sensitive to retrogression and better preserved throughout the SL complex. Several lawsonite types were identified in the LPU of the Cottian Alps by Lefeuvre et al. (2020) and can be recognized across the entire SL complex. We hereafter use the abbreviations defined in Lefeuvre et al. (2020): (1) LwsA are mostly found in pelitic calcschists as dark prismatic crystals filled with inclusions of organic matter; (2) LwsB consist of cream-coloured elongated fibers with long axis parallel to the vein walls and aligned with quartz crystals ± minor ankerite; LwsB occurs in pluri-centimetric to metric veins subparallel to the present schistosity (Figs. 4b, c, e); (3) LwsC co-crystallizes with quartz and ankerite as cream-coloured fibers perpendicular to the walls of mm- to cm-large tensile veins (Figs. 4d, f). While LwsA crystals in the host calcschists formed early on during prograde metamorphism, several generations of LwsB- and LwsC-bearing veins appear to have formed along the prograde P-T path up to peak burial depths, through dissolution-precipitation processes and lawsonite-forming reactions (Lefeuvre et al., 2020; Fig. 3).

Compared to metasediments, metamafic rocks from the SL complex are almost devoid of veins (Figs. 4g, h). Studies reporting direct evidence of fluid circulation during burial to peak conditions focused on (1) glaucophane shear-bands in BS-facies metagabbroic bodies (Schwartz, 2000; Debret et al., 2016), (2) omphacite-bearing veins in eclogite-facies rocks of Monviso and Rocciavre bodies (Philippot, 1987; Philippot and Kienast, 1989; Philippot and Selverstone, 1991; Philippot et al., 1998), (3) eclogitic breccias of Monviso (Angiboust et al., 2012a; Locatelli et al., 2018) and (4) kyanite-bearing veins in Zermatt-Saas eclogites (Fry and Barnicoat, 1987; Widmer and Thompson, 2001).

In Monviso, brecciated Fe-Ti-metagabbros crop out in major shear zones (Intermediate and lower shear zones; Angiboust et al., 2012a, Locatelli et al., 2018). Different generations of veins and eclogitic breccia matrices were characterized (Locatelli et al., 2018) (1): the first

generation of vein (V1) and matrix (M1) is almost exclusively composed of omphacite whereas (2) the second generation of vein (V2) and matrix (M2) is filled by omphacite and garnet; (3) the last matrix generation (M3) is composed of lawsonite pseudomorphs and relics of garnet and omphacite. Thermodynamic modelling and trace elements analysis of omphacite and garnet in these veins and matrices allowed to identify the progressive opening of the system to external fluid infiltrations (Locatelli et al., 2018, 2019b): from metric at peak conditions (V1 veins and M1 matrix) to possibly decametric opening at early retrograde conditions (V2 veins and M2) and hectometric to kilometric opening at retrograde conditions (M3).

3.2. HP veins and sampling along the Queyras-Monviso traverse

Outcrops were selected across the LPU1, LPU2, LPM and LPL units of the Queyras-Monviso traverse (Table 2). HP veins can locally reach around 20-25 vol% of the outcrop (Fig. 4a). Fresh lawsonite-bearing veins were found in LPU1, LPU2 and LPM, and creamy-colored lawsonite crystals were observed in both LwsB (Figs. 4b, c, e) and LwsC veins (Figs. 4d, f). The abundance of lawsonite-bearing veins strongly depends on lithology (see Lefeuvre et al., 2020): they are much more abundant in calcschists containing roughly similar amounts of pelites and carbonates in fine alternations than in carbonate-dominated host rocks (where only calcite ± ankerite veins are present). LwsB-bearing veins are abundant in LPU1, but far less abundant than LwsC tension gashes in LPU2 and LPM.

Fewer Fe-Mg carpholite-bearing veins were observed along this the traverse (which is more carbonate-rich than that of the Cottian Alps) and only one sample containing carpholite needles in a syn-foliation quartz vein from LPU1 was collected. Chloritoid is present across most of LPM, showing that carpholite is not stable anymore (Fig. 3; as for the Cottian Alps: Agard et al., 2001; Bebout et al., 2013). By comparison with BS-facies metasediments, eclogite-facies metasediments lack diagnostic veins and/or show strongly transposed veins so that no clear example of peak burial vein could be found in these rocks.

BS-facies metagabbro bodies exhibit jadeite-rich clinopyroxene-bearing peak assemblages, i.e. lawsonite-jadeite-glaucophane in LPU1 and zoisite-jadeite-glaucophane in LPM (Saliot, 1979; Schwartz, 2000; Tricart and Schwartz, 2006) and cm-scale jadeite-veins that could be sampled (Fig. 4g). In eclogite-facies metamafics, we used samples of omphacite ± garnet bearing veins (Fig. 4h) and matrices of eclogitic breccias from Monviso massif of LPL unit (see Locatelli et al., 2018; 2019b).

Outcrops 1 to 4 belong to LPU1 and correspond to metasediments (Fig. 2b, Table 2; 1: east of Château-Queyras; 3: between Ville-Vieille and Aiguilles, Malafosse locality; 4: between Aiguilles and Abriès, Le Gouret locality), except for the outcrop 2 lawsonite-jadeite-glaucophane-bearing metagabbro block (west of Ville-Vieille, close to Guil river). LPU1 samples comprise LwsB- and LwsC-bearing veins (outcrops 1, 3 and 4), one jadeite-bearing vein (outcrop 2) and one carpholite-bearing vein (outcrop 3).

Outcrops 5 and 6 belong to LPU2 (Fig. 2b, Table 2; 5: vallée de la Blanche, near Clausis chapel; 6: bottom of Pain de Sucre, near Col Agnel) and correspond to LwsB- and LwsC-bearing veins in metasediments.

Outcrops 7 to 9 belong to LPM (Fig. 2b, Table 2; 7: Pelvas d'Abries, Col d'Urine; 8: Col Bouchet; 9: between Refuge du Viso and Col Valanta). LPM samples comprise LwsB- and/or LwsC-bearing veins in metasediments (outcrops 8 and 9) and one jadeite-bearing vein (outcrop 7).

Outcrops 10 and 11 belong to LPL (Fig. 2b, Table 2; 10: Intermediate Shear Zone, near Lago Superiore; 11: Lower Shear Zone, east of Rifugio Quintino Sella). Both correspond to Fe-Ti metagabbro blocks metamorphosed, mylonitized and brecciated under eclogite-facies conditions. Omphacite-bearing veins V1 and V2 (see Locatelli et al., 2018; 2019b) crosscutting the mylonitic foliation and M2 matrix of eclogitic breccias were sampled in outcrop 10. M1 matrix of eclogitic breccias was studied in outcrop 11.

4. Analytical strategy and methods

4.1. Fluid Inclusion micro-textural analysis and selection.

Fluid inclusion (FI) analyses were performed on 100 µm thick double-polished sections. FI were observed using optical microscopy, in order to characterize their morphology, gas/liquid ratios and textural location within crystals. To characterize the pristine fluids present during crystal growth, only fluid inclusions showing good textural evidences of primary entrapment were selected (Figs. 5 a-f; i.e., fluid inclusions either isolated or in non-planar clusters inside mineral grains; Roedder, 1994; Van den Kerkhof and Hein, 2001). The FI were carefully examined and we selected inclusions with the most regular shapes in order to avoid as much as possible post-entrapment modification of FI chemistry. FI aligned on trails crosscutting several mineral grains, considered as secondary inclusions in recrystallized fractures, were not considered in this study.

4.2. Fluid salinity: microthermometric versus Raman spectroscopy measurements

Microthermometric measurements were carried out on a subset of quartz and omphacite fluid inclusions at ISTeP (Sorbonne Université) using an optical microscope equipped with a Linkam THMSG600 heating-freezing stage (-196 °C to +600 °C) controlled by a Linkam TMS-93 programmer via LinkSys software v.2.15. Ice melting and liquid-vapor homogenization temperatures were reproducible within 0.1 °C (~0.2 wt.% NaCl eq.) and 1 °C, respectively. Salinity was estimated from ice-melting temperatures using the equation of Bodnar (1993). Eutectic temperatures were also measured in FI from omphacite veins, in which a complex salt system was assumed. Values are reported in Sup. mat. 1.

In the studied samples, homogenization temperatures (Th) showed a large scatter, suggesting density reequilibration of FI due to deformation during exhumation (Vityk and Bodnar, 1995a, 1995b; Bodnar, 2003b; Diamond, 2003; Tarantola et al., 2012; Raimbourg et al., 2018), as already observed in fluid inclusions trapped in HP conditions in the SL complex (Agard et al., 2000; Philippot and Selverstone, 1991). Th and density measurements were not further performed since our study focuses on fluid compositions and such data would have been meaningless.

Ice-melting temperatures (Tm_{ice}) were difficult to obtain for most FI due to their small size (most FI <10µm), and only few Tm_{ice} measurement were obtained in Monviso omphacite due to the FI thick walls and stretched, motionless gas bubbles. This resulted in a very limited number of salinity data for most samples.

Salinity can also be determined by Raman spectroscopy with an accuracy of ± 0.4 wt% NaCl eq., owing to recent calibrations performed at GeoRessources laboratory (Université de Lorraine, Nancy; Caumon et al., 2013, 2015; Tarantola and Caumon, 2015) as the Raman spectrum of liquid water in the OH stretching vibrations is a function of salinity (Fig. 6). Raman spectroscopy data of our FI set were collected with the very same spectrometers used for calibration in the works above (see 4.3). Salinities measured by both microthermometry and Raman spectroscopy for a subset of samples (Sup. mat. 1; Fig. 7) are similar within the sum of the respective uncertainties of each method (0.6 wt% NaCl eq.): they plot on the 1:1 line in figure 7, showing the validity and good accuracy of Raman spectroscopy for salinity measurements in our samples. This further shows that Raman spectroscopy can be confidently used to determine salinity in all our FI, which enables acquiring a statistically robust dataset for a large number of samples (445 FI studied in 22 samples).

4.3. Raman spectroscopy for salinity, gas and mineral analysis.

Most studied FI are two-phase (liquid-vapor) and only some contain daughter mineral phases (three-phase inclusions). Salinity, gas content and nature of daughter minerals of the 445 studied FI were determined by Raman spectroscopy, by focusing the laser on the liquid phase, gas bubble and minerals respectively. Raman measurements were performed at GeoRessources laboratory (Université de Lorraine, Nancy) using a LabRAM HR and a LabRAM spectrometer (Horiba Jobin-Yvon®) equipped with a liquid nitrogen-cooled CCD detector, a 600 groove.mm^{-1} grating for salinity measurements and a 1800 groove.mm^{-1} grating for gas analysis. The excitation light was provided by an Ar$^+$ laser (Stabilite 2017, Newport Spectra-Physics) at 514.532 nm at a power of 200, 160 or 120 mW, focused on the sample using a 100x objective (Olympus).

Salinities were determined using the method described in Caumon et al. (2013, 2015) and Tarantola and Caumon (2015). Raman spectrum of water in the studied FI were acquired and salinity were determined using the intensity ratio of two defined positions (3260 and 3425 cm^{-1}) after subtraction of a linear baseline.

For gas analysis, Raman spectra were corrected using an ICS function (Intensity Correction System) to normalize the instrument response with wavelength. Gas spectra were identified using peak positions compiled by Frezzotti et al. (2012). CO_2 was detected by the presence of the Fermi diad (Fermi, 1931; 1285 and 1388 cm^{-1} peaks, Fig. 8a), CH_4 by the major band at 2917 cm^{-1} (Fig. 8a) and N_2 by the major band at 2331 cm^{-1} (Fig. 8b). Presence of N_2 in the inclusion was then confirmed by subtraction of the atmospheric N_2 peak area on the main band of N_2 detected in inclusion. For CO_2-CH_4 mixtures, peak areas were computed after substraction by a linear baseline. Molar proportions of each gas in the mixtures were determined using the respective area and the corresponding relative Raman scattering cross-section (RRSCS; Wopenka and Pasteris, 1987). We choose to use the recent values of Le et al. (2019, 2020) for RRSCS of CO_2 (1.40 ± 0.03 for the 1388 cm^{-1} peak and 0.89 ± 0.02 for the 1285 cm^{-1} peak) and CH_4 (7.73 ± 0.16 for the major band at 2917 cm^{-1}).

Daughter minerals were identified using the data compilation of Frezzotti et al. (2012).

5. Petrography and microstructural analysis of fluid inclusions

Lawsonite-bearing veins (LPU1-LPU2-LPM)

All studied samples of LwsB-bearing veins contain idiomorphic-fibrous crystals of lawsonite. These fibers are parallel to the vein walls, generally several cm-long and mm-thick and always exhibit fine alternation with quartz fibers and commonly ankerite (Figs. 5a, b). Lawsonite is frequently pseudomorphed in the veins by fine-grained assemblages of phengite, chlorite and calcite, as previously reported (Sicard-Lochon, 1987; Vitale Brovarone et al., 2014; Lefeuvre et al., 2020). Similar features are observed in LwsC-bearing veins except that fibers are smaller, more often replaced by the late-greenschist facies assemblage (phengite, chlorite, calcite) and ankerite is always present in apparent equilibrium with quartz and LwsC fibers.

FI were systematically studied in quartz co-crystallizing with lawsonite ± ankerite fibers (Figs. 5a-c). Although FI are commonly very densely packed, hampering a correct assessment of their primary or secondary nature (Fig. 9a), some are found in quartz grain cores as isolated inclusions or in non-planar-clusters indicating primary entrapment. Inclusion sizes are 5-15 μm and rarely reach 20 μm. These inclusions are mostly two-phase (L+V; Figs. 9b, c) with a vapor bubble occupying typically ~10-20% of the inclusion volume. These inclusions commonly show a well-defined slightly elongate shape (Figs. 9b-e), but some exhibit angular shapes suggesting post-entrapment modification (Fig. 9d). A small number of isolated primary FI are monophase (L), suggesting metastability. Out of over 250 FI from lawsonite-bearing veins, only four (all from sample 1LwsB) are three-phased (L+V+S), with two of them containing a cubic highly-refractive crystal (Fig. 9e).

Carpholite-bearing veins (LPU1)

In the carpholite–bearing sample (outcrop 3), almost all carpholite crystals are replaced by retrograde chlorite. Preserved fresh carpholite occurs as needle clusters in quartz, highlighting co-crystallization of carpholite and quartz during BS-facies conditions (Figs. 5d-f).

FI were only characterized in quartz crystals hosting carpholite needles (Fig. 5f) and are very similar to those of lawsonite veins. Primary FI are biphase (L+V), 5-20 μm in size and occur as isolated or in non-planar clusters (see also Agard et al., 2000). The vapor bubble also represents ~10-20% of the inclusion volume, and the FI generally have regular shapes.

Jadeite-bearing veins (LPU1 and LPM)

Jadeite-bearing veins are composed of jadeite idiomorphic green crystals with multiple orientations (Fig. 9f) and few glaucophane crystals generally filling fractures.

FI have a well-defined tubular shape and are generally small in 2Jd sample (LPU1, a few micrometers, rarely up to 20 μm), while slightly bigger in 7Jd sample (LPM, 5-20 μm in size,

rarely up to 25 μm). All these inclusions are systematically oriented parallel to the c-axis of jadeite crystals and occur as isolated or in non-planar clusters (Fig. 9f), suggesting primary entrapment. These inclusions are generally biphase (L+V) but few monophase (L), biphase (L+S; 2/23 in 2Jd) or triphase FI (L+V+S; 2/23 in 2Jd) were identified. The vapor bubble generally occupies ~5-10% of the inclusion total volume in 2Jd sample and ~20% in 7Jd sample.

V1 and V2 omphacite (± garnet) bearing veins (LPL)

V1 veins are almost parallel to the eclogitic foliation. They are filled by pluri-millimeter-long fibrous and euhedral omphacite crystals. These crystals are generally oriented perpendicular to the vein walls and show concentric-zoning. V2 veins are filled with omphacite and garnet. Garnet is idiomorphic, mm-sized, while omphacite crystals are slightly smaller than in V1 veins.

In both vein types, most primary FI are concentrated in the core of omphacite crystals, to which their dense clustering gives a darkish color (Fig. 9g). These inclusions occur as isolated or in non-planar clusters. They are tubular-shaped, typically 10-20 μm large and up to ~40 μm, and are always oriented parallel to the c-axis of omphacite (Figs. 9h, i). There are as many biphase (L+V) as triphase (L+V+S; Figs. 9h, i) inclusions, and the vapor bubble generally occupies 15-20% of the inclusion total volume. Triphase inclusions generally contain one or several transparent anisotropic solids and some a cubic-shaped darkish-colored opaque solid. In many of these inclusions, material recrystallized on the inclusion borders, creating thick internal walls that squeeze the (often elongate) gas bubble. The refraction index suggests it could be omphacite.

M1 omphacite-bearing and M2 omphacite-garnet-bearing matrices (LPL)

M1 matrix of Monviso eclogitic breccias is almost entirely made of light-green idiomorphic crystals of omphacite with minor apatite, while M2 matrix is dominantly composed of euhedral omphacite crystals with idiomorphic zoned garnets.

In M1 matrix, FI are isolated or in non-planar clusters and oriented parallel to the omphacite-c axis, again suggesting primary entrapment. Most inclusions are 5-10 μm sized, generally biphase (L+V) and rarely triphase (L+V+S; 5/24), containing a colorless solid. The vapor bubble has an almost constant volume representing 10-15% of the inclusion total volume.

M2 matrix primary FI are relatively similar: 5 to 15 μm in size, rarely 20 μm, parallel to the omphacite c-axis. These inclusions are biphase (L+V) and only two triphase (over 19; L+V+S) were observed, one with an opaque solid, the other with a colorless solid. The vapor

bubble generally occupied ~10% of the inclusion total volume. As for the omphacite-bearing veins, some inclusions expose thick walls of recrystallized material.

6. Fluid inclusion chemistry

276 FI from metasedimentary veins, 43 FI from BS mafic samples and 126 FI from eclogitic mafic samples were analyzed by Raman spectroscopy to determine fluid salinity, gas content and the nature of daughter minerals.

6.1. Fluid inclusion salinity

Lawsonite and carpholite veins (LPU1, LPU2 and LPM)

The fluid salinity estimated in primary FI from lawsonite-bearing quartz veins generally shows low to intermediate salt concentrations (mean: 4.8 wt% NaCl eq.; median: 3.2 wt% NaCl eq.) and fairly variable values (standard deviation sd: 4.1). Detailed salinity values for lawsonite-bearing veins in each outcrop are (mean; median; sd; in wt% NaCl eq and FI numbers): outcrop 1 (11 wt%; 7.8 wt%; 8.1; n = 34), outcrop 3 (1.8wt%; 1.8wt%; 1.4; n = 33); outcrop 4 (6.4wt%; 6.3wt%; 3.2; n = 44); outcrop 5 (8.1wt%; 3.9wt%; 5.8; n = 44); outcrop 6 (2.8wt%; 2.6wt%; 2.3; n = 44); outcrop 8 (4.3wt%; 3.2wt%; 4.1; n = 14) and outcrop 9 (1.2 wt%; 0.9 wt%; 1.2; n = 41). No obvious salinity difference between LwsB- and LwsC-bearing veins was detected in any sample. The carpholite-bearing sample from outcrop 3 has a low-salinity range similar to the lawsonite-bearing samples from the same outcrop (2.4 wt%; 2.7 wt%; 1.5; n = 22).

Since a clear eastward increase in metamorphic grade is observed along this traverse (Fig. 3), measured salinities are presented as a function of longitude (Fig. 10a). Vein salinities in metasedimentary rocks show a decreasing trend of average salinity towards the east, from outcrop 1 (11 wt% NaCl eq.) to outcrop 9 (1.2 wt% NaCl eq.). This trend is further illustrated in Figs. 10b-d, where salinity data are represented in cumulative bar-charts for each unit. In each chart, salinities follow an approximate normal Gaussian distribution truncated at low values and show a decreasing salinity trend at the unit scale, from LPU1 (5.8 wt%; 4.2 wt%; 5.8; n = 133) to LPU2 (4.4 wt%; 3.1 wt%; 4,68; n = 88) and to LPM (2.0 wt%; 1.3 wt%; 2.63; n = 55). In LPU1, FI salinity is highly variable (sd: 5.8), particularly for outcrop 1 where salinities are frequently above 10 wt% NaCl eq. and even >25 wt% NaCl equivalent. Measured salinities for this unit are generally above early Cretaceous seawater salinity (~

3.2-3.7 wt%; Hay et al., 2006), whereas in LPU2 and LPM salinities are mostly close or lower to seawater salinity.

Jadeite-bearing veins (LPU1 and LPM)

In BS-facies jadeite-bearing veins, FI salinity is generally higher than in surrounding metasediments (16.4wt%; 11.8 wt%; 9.4; n = 43). Intermediate values of salinity are found for 2Jd sample from LPU1 (Figs. 10a, b; 9.1 wt%, 9.1wt%; 2.8; n = 23), while fluid salinity is higher in 7Jd sample from LPM (Figs. 10a, c; 24.6 wt%. 28.4wt%; 7.1; n = 20).

V1 and V2 omphacite (± garnet) bearing veins (LPL)

Eclogite-facies omphacite-bearing veins from LPL share similar salinity ranges. These salinities are intermediate to high for both V1 (Figs. 10a, e; 14.6 wt%; 13.3wt%; 5.4; n = 37) and V2 (Figs. 10a, e; 14.6 wt%; 14.8 wt%; 4.1; n = 46).

Eutectic temperatures measured in 10OmpV1 sample range from -22.0 °C to -24.3 °C (Sup. mat. 1). These temperatures are lower than pure H_2O-NaCl eutectic temperature (-21.2 °C) and close to H_2O-NaCl-KCl eutectic temperature (-22.9 °C; Bodnar, 2003a), suggesting the presence of both NaCl and KCl. Minor presence of $MgCl_2$ and/or CaCl2 could account for the lowest eutectic temperatures (eutectic temperatures: H_2O-NaCl-$MgCl_2$: -35 °C; H_2O-NaCl-CaCl$_2$: -52 °C; Davis et al., 1990; Bodnar, 2003a).

M1 Omphacite-bearing and M2 omphacite-garnet-bearing matrices (LPL)

As in omphacite-bearing veins, salinity of fluids trapped in matrices from eclogitic breccias are clearly higher than seawater salinity, with high values for both M1 (Figs. 10a, e; 26.4 wt%; 27.2 wt%; 2.6; n = 24) and M2 matrix (Figs. 10a, e; 18.9 wt%; 17.4 wt%; 4.6; n = 19).

6.2. Fluid inclusion gas content

BS-facies metasediments: lawsonite- and carpholite-bearing veins

In FI vapor bubble from metasedimentary veins, the two peaks constituting the fermi diad of CO_2 (1285 cm^{-1} and 1388 cm^{-1}) and the 2907 cm^{-1} peak of CH_4 were identified in most of our inclusions and a Raman signal strong enough to make quantitative measurements was obtained in 110 FI. The molar proportion of each gas in the CO_2-CH_4 gas mixtures is represented according to FI salinity (Fig. 11). LwsC-bearing vein FI generally contain proportionnaly more CH_4 in CO_2-CH_4 mixtures (CO_2%; Mean: 29.4%; Med: 25.4%; n = 44) than in LwsB- (CO_2%; Mean: 67%; Med: 82%; n = 57) and carpholite-bearing veins (CO_2%;

Mean: 88.1%; Med: 90.4%; n = 9). Contrary to salinity, gas ratios do not show any particular correlation with P-T conditions.

In very few FI from LPU2 Lws-bearing veins (2 FI over 46 analyzed in 5LwsB and 5LwsC samples), several peaks were identified in the 2800-3000 cm^{-1} region (Fig. 12). These peaks correspond to the symmetrical and asymmetrical stretching vibrations of CH_2 and CH_3. These spectra, exclusively detected inside fluid inclusions, were carefully compared to the Raman spectra of the glue and oil used for sample preparation (Sup. mat. 2) and showed systematically different patterns. Distribution of peak positions corresponds to saturated hydrocarbons and fits well with pentane spectra (Sterin et al., 1980). These FI, visually identical to the aqueous ones (biphase, L+V), thus contain potential liquid and gaseous hydrocarbons (HC) heavier than CH_4 without any detectable trace of water or other gas species.

BS-facies metamafics: jadeite-bearing veins

In jadeite-bearing vein samples from LPU1 and LPM, no gas (other than H_2O vapor) was detected in the vapor bubble of aqueous inclusions. Nevertheless, potential hydrocarbon spectra similar to those of Lws-bearing veins were detected in 3/26 FI of 2Jd sample (LPU1) and in 5/24 FI of 7Jd sample (LPM). These hydrocarbons were identified in monophase (L) and few biphase (L+S) inclusions.

Eclogite-facies metamafics: omphacite-bearing veins and matrices

N_2 was frequently detected in omphacite-bearing veins V1 (in 10/17 FI) and V2 (in 18/29 FI), in particular in triphase (L+V+S) and in few biphase (L+V) inclusions. N_2 was similarly detected in M2 matrix (in 5/13 FI) in the biphase and the only triphase inclusions. Conversely, no gas (other than H_2O) was detected in the bubble of analyzed aqueous FI from M1 matrix.

6.3 Solids in fluid inclusions

In Lws-bearing veins, only four FI, all from 1LwsB and showing very high salinity (i.e. salinity exceeding NaCl-saturation value in water at room temperature), contain solids. Calcite was identified by Raman analysis in two of them. The other two FI contain colorless solids undetectable by Raman spectroscopy, with a cubic habit resembling that of salt crystals, which is in good agreement with the high salinity determined for these inclusions. We posit that these solids are daughter minerals formed by fluid supersaturation with respect to salts under post-entrapment decreasing P-T conditions. Similar crystals probably failed to nucleate due to metastability in the other rare high salinity inclusions of this sample (Bodnar, 1994, 2003a).

In Jd3 bearing-sample, calcite was detected in two aqueous FI and a white mica was detected in one aqueous FI and one HC-rich FI. These solids were only found in rare inclusions and are not systematically present in all FI of a cluster. Such crystals are regarded as having formed by post-trapping reactions between the fluid and the host mineral.

In omphacite-bearing veins and matrices from Monviso, Raman spectra of the FI thick walls are systematically similar to host omphacite spectra but with different peak intensity ratios, which suggests that these walls are made of omphacite with different orientations, ie. omphacite recrystallized during decreasing P-T conditions. About half of the FI from V1 and V2 veins contain solids, calcite being the more common (19 occurrences). Calcite was frequently detected in clustered FI with similar phase ratio (liquid/gas/solid) suggesting that these solids are daughter minerals. White micas were detected in three calcite-bearing inclusions in these veins and could have formed by post-trapping fluid-host mineral reactions. Opaque cubic solids (7 occurrences in calcite-bearing FI) could not be identified because they were systematically too mobile under the laser. These opaque solids could have formed by post-trapping fluid-host mineral reactions, or were accidentally trapped in these inclusions. An opaque solid was also detected in one FI from M2 matrix and calcite detected in two FI from M1 matrix. Finally, in 12 FI, colorless solids remained undetected by Raman spectroscopy. Such crystals are very small and may have too low Raman signals to be detected. However, most of them occur in highly-saline FI (i.e., salinity close to or exceeding salt-saturation values in water at room temperature) from omphacite-bearing matrices and veins, and could therefore be salt crystals. However, during microthermometric measurements, none of these crystals could be dissolved in FI even at temperatures about 450-500 °C.

7. Discussion

7.1. Validity of salinity data

7.1.1 Possible origin for salinity variations

Salinity data appear homogeneous for some localities (e.g., #3, 6, 9) but exhibit large variations in others, in both metasediments (e.g., LPU1: 1LwsB, 1LwsC; LPU2: 5LwsB, 5LwsC; Figs. 10a-c) and metamafics (localities #7,10; LPM and LPL; Figs. 10a, e). Such variations may either reflect sequential trapping during vein growth of fluids with variable salt concentrations or post-entrapment modification of inclusions. Although the least deformed lawsonite-bearing HP veins were sampled, some quartz crystals in metasediments may have been slightly deformed during retrograde exhumation (D2, D3). This process affects fluid

inclusion shape and density, but chemistry is supposed to be largely preserved, at least for intact FI (Diamond et al., 2010).

However, partial leakage of fluid inclusions with preferential release of small amounts of H_2O (i.e., increasing salinity; Bakker and Jansen, 1990, 1991, 1994; Hall and Sterner, 1993) cannot be excluded, and could account for the few outliers with higher salinity in outcrops 2, 5 and 8. For outcrop 5, this interpretation is also supported by the slightly irregular shapes of high-salinity FI indicating potential partial leakage, whereas FI with clustered salinities have a more regular shape. In contrast, the large salinity range observed for outcrop 1 is difficult to explain by post-entrapment partial leakage only since most fluid inclusions show regular shapes, even for LwsC vein high-salinity data, and rather suggests entrapment of a variably saline fluid. Note that as we only analyzed FI with the most regular shapes, the link between FI morphology and potential partial leakage is however too weak to allow discarding any outlier. All data are thus considerd in Fig. 10a-e.

In mafic outcrop 10 from Monviso LPL, all vein and matrix generations show large salinity ranges (Fig. 10e). The absence of macroscopic deformation of vein and matrix omphacite and the higher salinities reported for low-strained omphacite, compared to mylonitic omphacite of the surrounding rock (Nadeau et al., 1993), likely discard a systematic deformation-induced salinity increase in FI.

7.1.2 Validity of Raman salinity measurements

A few FI from Monviso LPL veins and matrices nevertheless contain colorless crystals undected by Raman spectroscopy, that could be salt crystals, but could not be dissolved in the liquid phase even at temperatures of 450-500 °C. This was also observed on similar Monviso omphacite vein FI by Philippot and Selverstone (1991) and Nadeau et al. (1993), who reported FI decrepitation at about 500°C before any dissolution of daughter crystals. If these crystals are salts, these FI could have experienced deformation-induced salinity increase and their present-day salinities would be underestimated by Raman measurements, which indicate the salinity of the fluid coexisting with the salt crystal.

Crystallization of other secondary phases in FI during exhumation could also account for changes in fluid salinity (Frezzotti and Ferrando, 2015). Indeed, most fluid inclusions in eclogitic veins and matrices are coated by thick walls of material crystallized from the fluid, reflecting decreasing mineral solubility with decreasing P-T conditions. The refraction index and Raman analyses suggest that most of this coating could be newly-formed omphacite, but a variety of other solids were also observed in these fluid inclusions, both in this study and a previous one on similar omphacite veins (Philippot and Selverstone, 1991). Such secondary

crystallization, in particular of H_2O-rich white mica, may slightly modify fluid inclusion salinity (Frezzotti and Ferrando, 2015).

In some FI, measured salinities exceed salt-saturation values in water at room temperature (Figs. 10a-e; salinities up to 30 wt.% NaCl eq., while saturation is at 23.2 wt.% NaCl eq.) although no salt crystal could be observed. This is true for most FI of mafic outcrops 7 and 11 and also concerns a few FI from mafic outcrop 10 and metasedimentary outcrops 1 and 5 (Figs. 10a-e). This could be explained by halite metastability in this salinity range. Indeed, halite hardly nucleates for salinities <30-35 wt.% NaCl, as shown by the restricted amount of microthermometrically-derived salinities in the 23-35 wt.% NaCl eq. range (Bodnar, 2003a) and may be sluggish in experiments even for salinities of 40 wt.% NaCl eq. (Bodnar, 1994). Such metastability was recently observed by Brooks et al. (2019) in FI from Sifnos, Greece.

Alternatively, the absence of salt nucleation may truly indicate that the fluid is not saturated with respect to any of the salt species. Salinities are indeed calculated from Raman-derived chlorinities in a simplified system, considering NaCl as the unique salt species. While NaCl is generally the dominant species, the presence of a variety of secondary minerals in FI from Monviso mafic samples (in veins in particular) suggests that the salt system could be much more complex. Eutectic temperatures measured for sample 10OmpV1 (Sup. Mat. 1) suggest the presence of both NaCl and KCl, with potentially minor amounts of $MgCl_2$ and/or $CaCl_2$. The presence of other salts was similarly inferred from the low eutectic temperatures measured in similar omphacite veins from Monviso (Philippot and Selverstone, 1991) and Rocciavre (Philippot et al., 1998)

7.2 Fluids in BS-facies metasediments: composition and potential sources

7.2.1 Local vs exotic source of fluid?

Lawsonite- and carpholite-bearing veins exhibit mostly low to moderate salinity aqueous fluids (in NaCl eq., mean 1.2-11 wt.%, med 0.9-7.8 wt%) with small amounts of CO_2 and CH_4 in the vapor phase of some fluid inclusions. CH_4 is commonly interpreted as formed by hydrocarbon cracking during prograde metamorphism (Mullis, 1979; Mullis et al., 1994; Mangenot et al., 2021) and is the dominant gas species recorded in low-temperature metasediments from accretionary wedges (Raimbourg et al., 2014, 2015, 2018; Vrolijk, 1987; Vrolijk et al., 1988; Sadofsky and Bebout, 2004). In contrast, CO_2 content tends to increase at higher temperatures (i.e., >270 °C, Mullis et al., 1994; Tarantola et al., 2007) and may become dominant over CH_4 below the brittle-ductile transition (Raimbourg et al., 2018). In the SL calcschists, CH_4 and CO_2 may be locally-derived, from the reduced carbonaceous

material of pelitic layers and from carbonate-rich horizons, respectively. CO_2 may in part form by oxidation of CH_4 (Tarantola et al., 2007, 2009), so that variations in the CO_2/CH_4 ratio among different veins may also reflect local changes in redox conditions depending on lithology (Tarantola et al., 2009; Cannaò and Malaspina, 2018).

Potential hydrocarbons heavier than CH_4 were identified in only two FI from metasediments, in both liquid and vapor phases from non-aqueous inclusions. Hydrocarbons are generally restricted to diagenetic conditions and undergo cracking during burial. However, liquid hydrocarbons (aromatic and aliphatic) and wet gas (C_2H_6) were found in primary FI from metamorphic minerals (quartz, calcite and lawsonite) in similar BS-facies metapelites from the Briançonnais and interpreted as preserved from metanogenesis during burial (Goffé, 1982; Goffé and Velde, 1984; Goffé and Villey, 1984). Hydrocarbons reported here may therefore have been trapped early during burial (thereby escaping cracking) and liberated later on during lawsonite formation as a phase immiscible with the local aqueous fluid, as attested by the absence of water in these inclusions. Alternatively, hydrocarbons may have formed by polymerization of methane trapped in inclusions (Kolesnikov et al., 2009).

Fluids analyzed in lawsonite- and carpholite-bearing veins present a wide range of salinities, from 1.2 to 11 wt.% NaCl eq. for mean values. Most outcrops record salinities close to or lower than seawater salinity (i.e., 3.5 wt.% NaCl eq. for modern seawater, 3.2-3.7 and up to 4.2 wt.% NaCl eq. for lower Cretaceous and upper Jurassic seawater, respectively; Hay et al., 2006), as for FI in metasedimentary sequences from accretionary wedges (Brantley et al., 1988; Smith and Yardley, 1999; Yardley and Graham, 2002; Sadofsky and Bebout, 2004; Rossetti et al., 2006; Raimbourg et al., 2014, 2015, 2018) and unsubducted sediments analogous to the SL metamorphic sediments (Helmintoïdes flysch, Fig. 13a; Raimbourg et al., 2018). Such salinities could reflect the mixing between seawater-like fluids initially present in sediment pores and grain boundaries with H_2O-rich fluid released upon dehydration during progressive burial (e.g., Raimbourg et al., 2015), hence advocating for locally-derived fluids.

In contrast, outcrops 1 and 4 of LPU1 show salinities greater than that of seawater, as previously reported for carpholite-bearing veins of upper SL units to the north and south of the study area (Agard et al., 2000; mean salinity ~9 wt% NaCl eq.). Outcrop 1 presents a particularly wide range of salinities, with high mean values (Figs. 10a, b; mean: 11 wt% NaCl eq.; med: 7.8 wt% NaCl eq.; sd = 8.1) and some FI above the salt-saturation threshold (up to 27 wt% NaCl eq.). While preferential H_2O-loss during post-entrapment leakage of FI could explain part of the highest salinity outliers (see § 7.1; Hall and Sterner, 1993), the large

scatter of salinities of outcrop 1 rather reflects trapping of fluids with variable salinity, either derived from compositionally distinct adjacent protoliths or far-travelled.

A potential hypothesis, to account for the higher salinity in the metasediments in LPU1, is the ingression of an external fluid derived from metamafics, as the latter rocks show higher salinities than metasediments (Figs. 10a-e). This hypothesis is nevertheless not relevant, as: i) LPU1 contains only few mafic bodies located far away from the studied outcrops and ii) where larger-scale and more abundant mafic bodies are found, as in LPM, metasediments trapped fluids with salinities lower than that of seawater (Figs. 10a-d). Fragments of Triassic Piemont metacarbonates embedded in LPU1 oceanic metasediments, which are found ~150 m away from outcrop 1 (Fig. 2b), are a more likely source of exotic fluids: these fragments regarded as former extensional allochtons (with a Briançonnais affinity) are commonly associated with evaporate-rich deposits akin to producing saline brines during prograde metamorphism. The mixing of variable amounts of infiltrating brines and locally-derived low-saline fluids could explain the wide salinity range of fluids trapped in the HP veins of LPU1 (Fig. 13c). FI from metamorphosed continental margins also generally exhibit higher salinity fluids than oceanic-derived accretionary sequences (Yardley and Graham, 2002).

Infiltration at prograde to peak burial depths, during the formation of Lws-bearing veins, by fluids derived from dehydrating fragments of Piemont units has tectonic implications for the past location of LPU1: this unit must have been located close to portions of the stretched continental margin units. Two alternative scenarios can be envisioned (Fig. 13b): (i) before tectonic slicing from the down going slab, the oceanic LPU1 was located next to the Briançonnais stretched continental margin and was subducted and detached from the slab last (Fig. 13b). It could even represent sequences directly deposited on a Triassic substratum (Lagabrielle, 1987); (ii) LPU1 was the unit furthest away from the Briançonnais margin but nevertheless contained extensional allochthons and/or olistostromes, such as the Piemont blocks to the west of LPU1 (Fig. 2b). In this case LPU1 would have been the first of the recovered units to have been subducted and detached from the slab, which would explain the tectonic stacking observed today more easily (Fig. 13b).

7.2.2 Salinity reduction with increasing grade?

In addition to local salinity variations, primary FI trapped in HP-LT metasedimentary assemblages show a trend of decreasing salinity with increasing burial depth: LPU1, LPU2 and LPM yield mean fluid salinities of 5.8, 4.4 and 2.0 wt.% NaCl eq. respectively (Figs. 10a-d). While the high salinities of LPU1 are at least in part lithologically-controlled, the salinity

decrease between LPU2 and LPM could reflect (i) a change in fluid salinity with increasing grade or (ii) initial protolith heterogeneities.

Heterogeneities in sediment compositions are common in SL metasediments and reflected by m- to hm-scale variations in carbonate versus pelitic contents (Fudral, 1996; Lagabrielle et al., 2015). Heterogeneous chlorine concentrations and isotopic values, interpreted as inherited from protoliths heterogeneities (Barnes et al., 2019), could explain some of the salinity variations observed between LPU1, LPU2 and LPM since Cl is highly fluid-mobile and directly controls salinity. Contrary to subducted metasediments of the Franciscan complex, whose decrease in bulk-rock Cl-content with increasing grade likely reflects the release of Cl-rich fluids during progressive dehydration (Catalina Schist, Barnes et al., 2019), no systematic change was detected in the SL complex, even at depth of partial destabilization of the main Cl-hosts (i.e., chlorite and white mica). This advocates for Cl retention in rocks, consistent with the release of a low-saline aqueous fluid such as observed in LPU2 and LPM.

Salinity decrease with increasing burial depth is nevertheless documented in the Franciscan complex (Sadofsky and Bebout, 2004) and attributed to the progressive dilution of initial seawater-like pore fluid by successive dehydration reactions releasing H_2O (Smith and Yardley, 1999; Yardley and Graham, 2002; Sadofsky and Bebout, 2004; Raimbourg et al., 2015). In the studied traverse, lawsonite is stable across grade and cannot contribute to fluid dilution: it starts forming early along the prograde path (~180 °C, LwsA type; Lefeuvre et al., 2020; Fig. 3) and keeps recrystallizing in veins with incremental deformation until peak burial (LwsB-C types). However, progressive dilution of fluid salinity by dehydration reactions is expected from the breakdown of water-rich Fe-Mg carpholite (~12 wt% H_2O; Agard et al., 2001; Bebout et al., 2013; Figs. 3; 13d), which occurs at the temperatures and depths reached in the eastern sector of LPU2 and in LPM. This hypothesis is supported by the fact that the lawsonite veins selected for this study, the freshest and least deformed hence formed close to the peak P-T conditions of each unit, sampled the deepest fluid compositions.

7.3 Fluids in BS- and eclogite-facies metamafics: composition and potential sources

7.3.1 Preservation of hydrothermal signatures?

In BS-facies metamafic blocks, FI in jadeite-bearing veins are dominantly aqueous with salinities higher than in the surrounding sediments (mean values: 9.1 in LPU1 and 24.6 wt.% NaCl eq. in LPM; Figs. 10a, b, d). High salinities are also recorded in fluids trapped in

omphacite-bearing veins and matrices from Monviso (17.5 wt.% NaCl eq.; Figs. 10a, e). The low eutectic temperatures associated to a variety of secondary minerals (calcite, white mica, salt crystals) as well as fluid salinities above the water NaCl-saturation threshold in some FI lacking salt crystals (see § 7.1) suggest entrapment of a various salt-rich fluid (NaCl-KCl ± minor amounts of $MgCl_2$ and/or $CaCl_2$) in BS- and eclogite-facies metamafics.

Similar highly saline fluids in omphacite-bearing samples from Monviso (vein and whole-rock; Philippot and Selverstone, 1991; Nadeau et al., 1993) and low-strain omphacite from Rocciavre (Philippot et al., 1998) were interpreted as inherited from hydrothermal alteration based on: (i) the similar $\delta^{18}O$ values (of pyroxene and whole-rock) in eclogites and hydrothermally altered crust, (ii) the similar δD of hydrothermal chlorite and amphibole in non-subducted mafic rocks (Chenaillet gabbros) and of omphacite in Monviso veins (Nadeau et al., 1993), (iii) the similarity between FI salinity and $\delta^{18}O$ signature of eclogitic veins and those of altered oceanic crust and unmetamorphosed ophiolites (Philippot et al., 1998).

Near-ridge high-temperature (> 500 °C) hydrothermal alteration of gabbros in reaction zones is classically accompanied by phase separation leading to the formation of brines (up to ~40-50 wt.% NaCl eq.) and vapor phases (e.g., Delaney et al., 1987; Kelley & Delaney 1987; Vanko, 1988; Nehlig, 1991; Kelley et al., 1992; Alt et al., 2010; Castelain et al., 2014; Verlaguet et al., 2020). In contrast to the upward migration of low-density vapor phases, less-buoyant brines may be stored at depth in gabbro porosity (Fontaine and Wilcock, 2006; Fontaine et al., 2007) and trapped as fluid inclusions in newly-formed amphibole (and epidote). Hydrothermal amphibole commonly hosts several tenths of wt% of Cl, and up to 4 wt% were analyzed in hydrothermal amphiboles from oceanic gabbros (Ito and Anderson, 1983; Vanko, 1986). Significant amounts of chlorine were found in amphibole from the Chenaillet ophiolite and in relict hydrothermal amphibole from LPU1 and LPU2 BS-facies metagabbros (up to 0.3 wt%; Debret et al., 2016).

During subduction of hydrothermally-altered gabbros up to BS-facies conditions, progressive breakdown of amphibole + plagioclase (± chlorite, epidote) to glaucophane + jadeite + lawsonite/zoisite will release only small fluid amounts (if any). The fluid released is expected to be Cl-rich, since glaucophane and lawsonite contain less Cl than hydrothermal amphibole (Debret et al., 2016), and may therefore have a high salinity. Mixing of this Cl-rich fluid with small volumes of brines released from amphibole FI could account for the high and variable salinity of BS-facies jadeite veins (Figs. 10a, b, d).

A much larger fluid release is expected during glaucophane and lawsonite breakdown to omphacite + garnet in eclogite-facies rocks (Fig. 3; Angiboust and Agard, 2010). This fluid probably has a lower salinity than that released under BS-facies conditions since

glaucophane and lawsonite contain only moderate amounts of Cl and brines provided by the final destabilization of relictual hydrothermal amphibole are volumetrically insignificant. The moderate salinity of some omphacite-bearing veins and matrices in Monviso (Figs. 10a, e) may reflect dilution of the high-salinity BS-facies fluid by progressive glaucophane breakdown into omphacite.

While no gas other than H_2O vapor was detected in BS-facies metamafics, N_2 is present in some FI from Monviso eclogites. N_2 is frequently detected in eclogite-facies FI (Andersen et al., 1989, 1990, 1993; Selverstone et al., 1992; Klemd et al., 1992; Mukherjee and Sachan, 2009) and generally interpreted as inherited from the breakdown of pre-eclogitic minerals hosting NH_{4+} (e.g., amphibole, feldspar). Ammonium, bound as NH_{4+} in K-Na-Ca-bearing minerals, was found in BS-facies metagabbros along the investigated SL traverse (Busigny et al., 2011). N_2 may therefore have been retained in glaucophane under BS-facies conditions (as NH_{4+} substituting for Na) and later released and trapped in FI when glaucophane broke down to omphacite under eclogite-facies conditions (Fig. 3).

The intermediate-to-high salinity and gas content detected in our FI in metamafics could therefore in part be inherited from variations in the degree of hydrothermal alteration predating subduction, thereby explaining the contrasts between samples (i.e., between 7Jd and 2Jd, or between Monviso outcrops 10 and 11; Figs. 10a, b, d, e). This conclusion is supported by the $\delta^{37}Cl$ and $\delta^{65}Cu$ signature of relictual hydrothermal amphibole, which attests to the preservation of the hydrothermal imprint throughout Alpine subduction (Busigny et al., 2011, 2018; Selverstone and Sharp, 2013).

7.3.2 Mixing with externally-derived fluids?

Several FI in BS-facies metagabbros contain potential hydrocarbons heavier than CH_4 without water, which did not mix with the local high-salinity fluid (i.e., eight FI in samples 2Jd and 7Jd, similar to the two FI in outcrop 5 lawsonite-bearing veins). This likely advocates for fluid infiltration from surrounding metasediments since metamafic rocks are generally devoid of organic matter (Fig. 13c). Dissolution and mobilization of carbonaceous material in the fluid was identified at metasediments-metamafics contacts in the SL complex (Vitale Brovarone et al., 2020b). Previous trace element and isotopic studies on these Queyras metamafic blocks furthermore argued for infiltration of volatiles from the surrounding metasediments (Lafay et al., 2013; Debret et al., 2016, 2018; Inglis et al., 2017). However, fluid infiltration from metasediments was probably limited, since mafic blocks and surrounding metasediments still have different salinities (Figs. 10a-e), and likely restricted to block rims and deformed zones (Schwartz, 2000, Debret et al., 2016), as suggested by the

preservation of rare magmatic pyroxene and hydrothermal amphibole in block cores (Philippot et al., 1998, Debret et al., 2016).

Hydrocarbons, whether or not derived from sedimentary fluids, could result from deep abiotic generation by polymerization of methane through a reversible reaction (forming ethane, propane, butane; Kolesnikov et al., 2009). Recent experimental and field data have suggested that CH_4 and other hydrocarbons can be stable at HP conditions and up to deep upper-mantle conditions (McCollom, 2013; Sverjensky et al., 2020; and references therein). Saturated hydrocarbons are formed in HP experiments by carbonate reduction (Tao et al., 2018) or transformation of dissolved organic species (Huang et al., 2017; Li, 2017). Immiscible abiotic CH_4 produced by carbonate reduction (Vitale Brovarone et al., 2017) and deep serpentinization (Vitale Brovarone et al., 2020a) was reported in HP ultramafic rocks from the Western Alps. Dissolved organic molecules, still present at UHP metamorphic conditions as shown by aqueous FI in deeply subducted metasediments (Frezzotti et al., 2011; Frezzotti, 2019), could also contribute to form hydrocarbons at BS-facies conditions.

Monviso Fe-Ti-metagabbros allow studying fluid ingression during progressive brecciation and strain localization at eclogite-facies conditions (Angiboust et al., 2012a; Locatelli et al., 2018). Thermodynamic modelling and trace element compositions suggest that omphacite crystallization in V1 veins and M1 matrix reflects final glaucophane and lawsonite breakdown in Mg-rich gabbros, while the omphacite from V2 veins and M2 matrix formed at incipient retrograde conditions without local fluid production and in the presence of some serpentinite-derived fluids (Locatelli et al., 2019b). The salinity of V2 and M2 omphacite FI does not deviate significantly, however, from that of V1 veins, suggesting either remobilization and entrapment of local remnant fluids (i.e., FI or grain boundary fluids) or that external fluid input was minimal (consistent with only incipient opening of the system; Locatelli et al., 2019b) and/or had a similar salinity. In ultramafic rocks, deserpentinization through the brucite-out reaction (as is the case in Monviso; Gilio et al., 2020) was shown to result in the formation of highly saline FI (Scambelluri et al., 1997), whereas the antigorite-out reaction produces less saline FI (Scambelluri et al., 2001).

7.4. Implications on fluid circulation during subduction of the SL complex

This study shows that salinities and gas signatures of HP metasedimentary FI can be accounted for by the progressive dilution of a local residual pore seawater-like fluid by successive dehydration reactions accompanying subduction. There is no strong evidence for infiltration of external fluids, except in LPU1 where high salinity fluids reflect hm-scale fluid circulation of brines from nearby Piemont blocks. This concurs with the conclusions from

whole-rock trace element and isotopic studies that SL metasediments represent a rock-buffered system with only limited external fluid infiltration (Henry et al., 1996; Bebout et al., 2013; Cook-Kollars et al., 2014; Barnes et al., 2019; Epstein et al., 2020).

Gas contents do not show systematic variations with increasing grade but the $CO_2/(CO_2\text{-}CH_4)$ ratio does with lawsonite vein type in all metasedimentary units (Fig. 11). In particular, LwsC crack veins reflecting cm-scale element transport from vein walls (Figs. 4d, f), mostly restricted to pelite-rich horizons, systematically contain higher CH_4 amounts. This suggests local fluid derivation from reduced carbonaceous material contained in pelites. Conversely, the larger LwsB-bearing veins (up to dm-wide, m-long; Figs. 4a-c, e) systematically higher $CO_2/(CO_2\text{-}CH_4)$ ratios suggest that the fluid produced by dehydration of pelitic horizons interacted with more distant carbonate layers, as also recorded by in-situ trace element signatures (Lefeuvre, 2020)

This spatial control on gas contents points to local variations of the redox state in the fluid, which hardly homogenizes at the m-scale. We interpret the small cm-scale LwsC tensile veins, which preserve their redox/CH_4-rich signature, as short-lived tectonic events accompanied by local fluid-rock interaction. In contrast, mass transfer and element redistribution across lithological horizons (Lefeuvre et al., 2020) could operate through fluid circulation in networks outlined by the larger-scale, longer-lived Lws-B veins, thereby explaining the calcite isotopic homogenization at the hm-scale (Henry et al., 1996; Cook-Kollars et al., 2014). There is however no evidence for larger scale infiltration of external fluid inside the SL units (Henry et al., 1996; Bebout et al., 2013; Cook-Kollars et al., 2014; Barnes et al., 2019; Epstein et al., 2020) and high fluid flow seems restricted to contacts between units (e.g., Jaeckel et al., 2018; Epstein et al., 2021). Although the presence of potential hydrocarbons hints towards element transfer between metasediments and metamafics, fluid circulations were probably more restricted in metamafic blocks, as suggested by the preservation of magmatic pyroxene in the undeformed cores of metagabbro blocks and locally-derived high-salinity fluids. This conclusion is strengthened by trace element data in metagabbros and serpentinites of the Monviso LPL unit, suggesting rather closed-system conditions upon burial and up to peak conditions (Spandler et al., 2011; Lafay et al., 2013; Locatelli et al., 2019b).

7.5. Comparison with other subduction zones

Fluid compositions trapped at peak burial in FI of the SL units are compared to those from other oceanic subducted fragments worldwide (Fig. 14; Table 1). Studies of shallow subduction depths mostly rely on metasediments (< 430 °C, about 20 kbar) whereas studies

of eclogite-facies conditions mostly do on metamafic samples (reflecting processes controlling rock recovery in subduction zones; Agard et al., 2018).

Similar salinity ranges and gas contents are recorded in trapped primary FI from BS-facies metasediments worldwide (Agard et al., 2000; Sadofsky and Bebout, 2004; Sachan et al., 2017; Raimbourg et al., 2018). Rather low-salinity fluids (< 5 wt% NaCl eq.) characterize low-grade to BS-facies metasedimentary rocks from accretionary wedges (Brantley et al., 1998; Smith and Yardley, 1999; Sadofsky and Bebout, 2004; Rossetti et al., 2006; Raimbourg et al., 2015, 2018). The evolution of fluid compositions in metasediments beyond BS-facies conditions remains uncertain due to only few studies. It may involve progressive dilution by locally-derived dehydration fluids, as observed in SL metasediments (this study) or in the Franciscan complex (Sadofsky and Bebout, 2004). Yet FI in Himalayan BS-facies metasediments record higher salinities (about 12 wt% NaCl eq.; Fig. 14; Sachan et al., 2017).

Metamafics from the various eclogitic terranes seem to be characterized by medium to highly saline primary FI (Luckscheiter and Morteani, 1980; Philippot and Selverstone, 1991; Selverstone et al., 1992; Nadeau et al., 1993; Philippot et al., 1998; Yoshida et al., 2015). They show a diverse set of solid inclusions (this study; Philippot and Selverstone, 1991; Selverstone et al., 1992), indicative of complex salt systems ($NaCl \pm KCl \pm CaCl_2 \pm FeCl_2 \pm MgCl_2$), and eclogites from oceanic and continental subduction commonly contain N_2 or CO_2 in the FI bubble (Andersen et al., 1990; Selverstone et al., 1992; El-Shazly and Sisson, 1999). Cogenetic monophase gaseous N_2-CO_2 $\pm$ CH_4-bearing FI were interpreted as representing immiscible fluids at peak burial conditions (Andersen et al., 1990; Andersen et al., 1993; Selverstone et al., 1992; Klemd et al., 1992; Mukherjee and Sachan, 2009).

FI from Alpine metagabbros are by far the most studied and record the highest salinities under both BS-facies and eclogitic conditions (10-45 wt% NaCl eq.; this study; Nadeau et al., 1993; Philippot and Selverstone, 1991; Philippot et al., 1998), reflecting at least partial inheritance from high-temperature amphibolite-facies hydrothermal alteration (Nadeau et al., 1993; Philippot et al., 1998). In comparison, ultramafic rocks having experienced antigorite breakdown above 600 °C exhibit lower salinity FI (Cerro de Amirez, Scambelluri et al., 2001) than only partially dehydrated serpentinites (Erro Tobbio, Scambelluri et al., 1997).

Localities outside the Alps (Fig. 14; e.g., Tianshan, Dominican Republic, Syros, Franciscan complex; Barr, 1990; Giaramita and Sorensen, 1994; Gao and Klemd, 2001; Kawamoto et al., 2018) record significantly lower fluid salinities (2-7 wt% NaCl eq.; Fig. 14), though still higher than for metasediments. Contrary to the Alpine case study, eclogites from the Franciscan complex, Samana Peninsula (Giaramita and Sorensen, 1994) and Rio San Juan

jadeitites (Kawamoto et al., 2018) correspond to mafic blocks in subduction mélanges (Agard et al., 2018): they may have experienced greater fluid circulation, thereby explaining the lower salinity values. In the Franciscan complex, eclogitic mafic blocks show slightly higher salinities than surrounding metasediments (Giaramita and Sorensen, 1994; Sadofsky and Bebout, 2004), suggesting that their initial fluid salinity was higher than that of the infiltrating sediment-derived (low-saline) fluids. Alternatively, since these mafic blocks are mostly metavolcanics they may have trapped initially low-salinity seawater-like fluids (Philippot et al., 1998): hydrothermalization of basalts indeed generally occurs under greenschist-facies conditions, preventing phase separation, brine trapping and formation of Cl-rich phases.

Conclusions

This study reports on salinities and gas contents of primary fluid inclusions (FI) trapped in high pressure veins from metasediments and metamafic rocks along the Queyras-Monviso traverse of the Schistes Lustrés complex (Western Alps). Results provide snapshots of fluids present at peak burial conditions from ~30 to 80 km depth, along a cold subduction zone.

Fluids trapped in metasediments are moderately saline aqueous fluids (mean salinity of 4.6 wt% NaCl eq.) with small amounts of CO_2 and CH_4 in the vapor phase. FI in metamafic HP veins record higher salinities (mean salinity about 17 wt% NaCl eq.) with small amounts of N_2 in eclogitic veins only, and a variety of daughter minerals (calcite, white mica, salts) indicative of complex chemical systems. These fluid signatures are consistent with literature data and appear characteristic of each rock type.

Salinity decreases with increasing grade in the studied metasediments, which is interpreted to reflect progressive dilution of initial seawater-like pore fluid by fresh fluids released locally by successive dehydration reactions. Higher salinities in the uppermost metasedimentary-dominated tectonic unit suggest brine infiltration from embedded continental margin fragments of former extensional allochtons, which are commonly associated with evaporate-rich deposits. CO_2 and CH_4 (and scarce potential hydrocarbons) appear to be locally released from fluid interaction with carbonates and carbonaceous matter-rich pelitic horizons, respectively.

In metagabbros, high salinities are interpreted as partly inherited from seafloor high-temperature hydrothermal alteration resulting in brine formation. Progressive breakdown of hydrothermal Cl-rich amphiboles to glaucophane (BS-facies) and then omphacite (eclogite-facies) and release of trapped FI brines could account for the high salinity fluids trapped in FI. Therefore, fluid inclusions record progressive release of Cl in the fluid phase with increasing grade.

FI in Alpine metasediments show salinities and gas contents comparable with other subducted fragments of oceanic lithosphere worldwide, whereas fluid salinities of Alpine metagabbros are higher than salinities recorded elsewhere. These higher salinities may result from (1) higher-temperature hydrothermal alteration and brine formation in Alpine metagabbros (compared to metavolcanics) or (2) more restricted infiltration by sediment-derived fluids compared to block-in-mélange subduction complexes.

This study suggests that fluids released in subduction zones from the different rock reservoirs are mostly aqueous but present variable salinities and gas contents. Characteristic local fluid signatures and redox conditions within units reflect restricted and transient fluid circulation. Conversely, lithological contrasts, often localizing fluid circulations, may take part in fluid mixing.

Supplementary data

Supplementary material 1: Comparison between microthermometry derived salinity and Raman salinity in the same inclusions and eutectic temperatures in Monviso omphacite vein.

Supplementary material 2: Comparison between the raman spectrum of the potential hydrocarbons and raman spectra of glue and oil used for sample preparation.

References

Agard, P., Goffé, B., Touret, J.L.R., Vidal, O., 2000. Retrograde mineral and fluid evolution in high-pressure metapelites (Schistes lustrés unit, Western Alps). Contributions to Mineralogy and Petrology 140, 296–315. doi.10.1007/s004100000190

Agard, P., Jolivet, L., Goffe, B., 2001. Tectonometamorphic evolution of the Schistes Lustres Complex; implications for the exhumation of HP and UHP rocks in the Western Alps. Bulletin de la Société Géologique de France 172, 617–636. doi.10.2113/172.5.617

Agard, P., Monie, P., Jolivet, L., Goffe, B., 2002. Exhumation of the Schistes Lustres complex: in situ laser probe 40Ar/39Ar constraints and implications for the Western Alps. Journal of Metamorphic Geology 20, 599–618. doi.10.1046/j.1525-1314.2002.00391.x

Agard, P., Yamato, P., Jolivet, L., Burov, E., 2009. Exhumation of oceanic blueschists and eclogites in subduction zones: Timing and mechanisms. Earth-Science Reviews 92, 53–79. doi.10.1016/j.earscirev.2008.11.002

Agard, P., Plunder, A., Angiboust, S., Bonnet, G., Ruh, J., 2018. The subduction plate interface: rock record and mechanical coupling (from long to short timescales). Lithos 320–321, 537–566. doi.10.1016/j.lithos.2018.09.029

Agard, P., 2021. Subduction of oceanic lithosphere in the Alps: selective and archetypal from (slow-spreading) oceans, Earth-Science Reviews, 103517.

Agard, P., Handy, M., 2021. Ocean subduction dynamics in the Alps, Elements, in press.

Alt, J.C., Laverne, C., Coggon, R.M., Teagle, D.A.H., Banerjee, N.R., Morgan, S., Smith-Duque, C.E., Harris, M., Galli, L., 2010. Subsurface structure of a submarine hydrothermal system in ocean crust formed at the East Pacific Rise, ODP/IODP Site 1256. Geochemistry Geophysics Geosystems 11. doi.10.1029/2010GC003144

Andersen, T., Burke, E.A.J., Austrheim, H., 1989. Nitrogen-bearing, aqueous fluid inclusions in some eclogites from the Western Gneiss Region of the Norwegian Caledonides. Contributions to Mineralogy and Petrology 103, 153–165. doi.10.1007/BF00378501

Andersen, T., Austrheim, H., Burke, E.A.J., 1990. Fluid inclusions in granulites and eclogites from the Bergen Arcs, Caledonides of W. Norway. Mineralogical Magazine 54, 145–158. doi.10.1180/minmag.1990.054.375.02

Andersen, T., Austrheim, H., Burke, E.A.J., Elvevold, S., 1993. N2 and CO2 in deep crustal fluids: evidence from the Caledonides of Norway. Chemical Geology 108, 113–132. doi.10.1016/0009-2541(93)90320-I

Angiboust, S., Agard, P., Jolivet, L., Beyssac, O., 2009. The Zermatt-Saas ophiolite: the largest (60-km wide) and deepest (*c.* 70-80 km) continuous slice of oceanic lithosphere detached from a subduction zone? Terra Nova 21, 171–180. doi.10.1111/j.1365-3121.2009.00870.x

Angiboust, S., Agard, P, 2010. Initial water budget: The key to detaching large volumes of eclogitized oceanic crust along the subduction channel? Lithos 120, 453-474.

Angiboust, S., Agard, P., Raimbourg, H., Yamato, P., Huet, B., 2011. Subduction interface processes recorded by eclogite-facies shear zones (Monviso, W. Alps). Lithos 127, 222–238. doi.10.1016/j.lithos.2011.09.004

Angiboust, S., Agard, P., Yamato, P., Raimbourg, H., 2012a. Eclogite breccias in a subducted ophiolite: A record of intermediate-depth earthquakes? Geology 40, 707–710. doi.10.1130/G32925.1

Angiboust, S., Langdon, R., Agard, P., Waters, D., Chopin, C., 2012b. Eclogitization of the Monviso ophiolite (W. Alps) and implications on subduction dynamics. Journal of Metamorphic Geology 30, 37–61. doi.10.1111/j.1525-1314.2011.00951.x

Angiboust, S., Pettke, T., De Hoog, J.C.M., Caron, B., Oncken, O., 2014. Channelized Fluid Flow and Eclogite-facies Metasomatism along the Subduction Shear Zone. Journal of Petrology 55, 883–916. doi.10.1093/petrology/egu010

Angiboust, S., Glodny, J., 2020. Exhumation of eclogitic ophiolitic nappes in the W. Alps: New age data and implications for crustal wedge dynamics. Lithos 356–357, 105374. doi.10.1016/j.lithos.2020.105374

Ballèvre, M., Lagabrielle, Y., Merle, O., 1990. Tertiary ductile normal faulting as a consequence of lithospheric stacking in the western Alps. Mémoires de la Société géologique de France 156, 227–236.

Ballèvre, M., Merle, O., 1993. The Combin Fault: compressional reactivation of a Late Cretaceous-Early Tertiary detachment fault in the Western Alps. Schweizerische Mineralogische Und Petrographische Mitteilungen 73, 205–227. doi.10.5169/SEALS-55570

Bakker, R.J., Jansen, J.B.H., 1990. Preferential water leakage from fluid inclusions by means of mobile dislocations. Nature 345, 58-60.

Bakker, R.J., Jansen, J.B.H., 1991. Experimental post-entrapment water loss from synthetic CO2-H2O inclusions in natural quartz. Geochimica and Cosmochimica Acta 55, 2215-2230.

Bakker, R.J., Jansen, J.B.H., 1994. A mechanism for preferential H2O leakage from fluid inclusions in quartz, based on TEM observations. Contributions to Mineralogy and Petrology 116, 7-20.

Barnes, J.D., Penniston-Dorland, S.C., Bebout, G.E., Hoover, W., Beaudoin, G.M., Agard, P., 2019. Chlorine and lithium behavior in metasedimentary rocks during prograde metamorphism: A comparative study of exhumed subduction complexes (Catalina Schist and Schistes Lustrés). Lithos 336–337, 40–53. doi.10.1016/j.lithos.2019.03.028

Barr, H., 1990. Preliminary fluid inclusion studies in a high-grade blueschist terrain, Syros, Greece. Mineralogical Magazine 54, 159–168. doi.10.1180/minmag.1990.054.375.03

Bebout, G.E., Agard, P., Kobayashi, K., Moriguti, T., Nakamura, E., 2013. Devolatilization history and trace element mobility in deeply subducted sedimentary rocks: Evidence from Western Alps HP/UHP suites. Chemical Geology 342, 1–20. doi.10.1016/j.chemgeo.2013.01.009

Bebout, G.E., Penniston-Dorland, S.C., 2016. Fluid and mass transfer at subduction interfaces—The field metamorphic record. Lithos 240–243, 228–258. doi.10.1016/j.lithos.2015.10.007

Beyssac, O., Goffé, B., Chopin, C., Rouzaud, J.N., 2002. Raman spectra of carbonaceous material in metasediments: a new geothermometer. Journal of Metamorphic Geology 20, 859–871. doi.10.1046/j.1525-1314.2002.00408.x

Blake Jr, M. C. (1988). Metamorphic and tectonic evolution of the Franciscan Complex, northern California. Metamorphism and crustal evolution of the Western United States, 1035-1060.

Bodnar, R. J., 1993. Revised equation and table for determining the freezing point depression of H2O-NaCl solutions. Geochimica et Cosmochimica Acta 57, 683–684.

Bodnar, R.J., 1994. Synthetic fluid inclusions: XII. The system H2O-NaCl. Experimental determination of the halite liquidus and isochores for a 40 wt% NaCl solution. Geochimica et Cosmochimica Acta 58, 1053–1063.

Bodnar, R.J., 2003a. Introduction to aqueous-electrolyte fluid inclusions, in Samson, I., Anderson, A., Marshall, D., 2003. Fluid inclusions: Analysis and Interpretation. Mineral Association of Canada, Short Course 32, 81-100.

Bodnar, R. J., 2003b. Re-equilibration of fluid inclusions, in Samson, I., Anderson, A., Marshall, D., 2003. Fluid inclusions: Analysis and Interpretation. Mineral Association of Canada, Short Course 32, 213-230.

Bousquet, R., Oberhänsli, R., Goffé, B., Wiederkehr, M., Koller, F., Schmid, S.M., Schuster, R., Engi, M., Berger, A., Martinotti, G. 2008. Metamorphism of metasediments at the scale of an orogen: a key to the Tertiary geodynamic evolution of the Alps. Geological Society, London, Special Publications 298, 393–411. doi.10.1144/SP298.18

Brantley, S.L., Fisher, D.M., Deines, P., Clark, M.B., Myers, G., 1988. Segregation veins: Evidence for the deformation and dewatering of a low-grade metapelite, in: Deformation-Enhanced Fluid Transport in the Earth's Crust and Mantle. pp. 267–288.

Brooks, H. L., Dragovic, B., Lamadrid, H. M., Caddick, M. J., & Bodnar, R. J., 2019. Fluid capture during exhumation of subducted lithologies: A fluid inclusion study from Sifnos, Greece. Lithos 332, 120-134.

Busigny, V., Cartigny, P., Philippot, P., Ader, M., Javoy, M., 2003. Massive recycling of nitrogen and other fluid-mobile elements (K, Rb, Cs, H) in a cold slab environment: evidence from HP to UHP oceanic metasediments of the Schistes Lustrés nappe (western Alps, Europe). Earth and Planetary Science Letters 215, 27–42. doi.10.1016/S0012-821X(03)00453-9

Busigny, V., Cartigny, P., Philippot, P., 2011. Nitrogen isotopes in ophiolitic metagabbros: A re-evaluation of modern nitrogen fluxes in subduction zones and implication for the early Earth atmosphere. Geochimica et Cosmochimica Acta 75, 7502–7521. doi.10.1016/j.gca.2011.09.049

Busigny, V., Chen, J., Philippot, P., Borensztajn, S., Moynier, F., 2018. Insight into hydrothermal and subduction processes from copper and nitrogen isotopes in oceanic metagabbros. Earth and Planetary Science Letters 498, 54–64. doi.10.1016/j.epsl.2018.06.030

Caby, R., Kienast, J.-R., Saliot, P., 1978. Structure, métamorphisme et modèle d'évolution tectonique des Alpes occidentales. Revue de géographie physique et de géologie dynamique Paris, 20, 307–322.

Cannaò, E., Malaspina, N., 2018. From oceanic to continental subduction: Implications for the geochemical and redox evolution of the supra-subduction mantle. Geosphere 14, 2311–2336. doi.10.1130/GES01597.1

Caron, J.-M., 1974. Rapports entre diverses" generations" de lawsonite et les deformations dans les Schistes lustres des Alpes cottiennes septentrionales (France et Italie). Bulletin de la Société Géologique de France 7, 256–263.

Cartwright, I., Buick, I.S., 2000. Fluid generation, vein formation and the degree of fluid-rock interaction during decompression of high-pressure terranes: the Schistes Lustrés, Alpine Corsica, France. Journal of Metamorphic Geology 18, 607–624. doi.10.1046/j.1525-1314.2000.00280.x

Castelain, T., McCaig, A.M., Cliff, R.A., 2014. Fluid evolution in an Oceanic Core Complex: A fluid inclusion study from IODP hole U1309 D—Atlantis Massif, 30°N, Mid-Atlantic Ridge. Geochemistry Geophysics Geosystems 15, 1193–1214. doi.10.1002/2013GC004975

Caumon, M.-C., Dubessy, J., Robert, P., Tarantola, A., 2013. Fused-silica capillary capsules (FSCCs) as reference synthetic aqueous fluid inclusions to determine chlorinity by Raman spectroscopy. European Journal of Mineralogy 25, 755–763. doi.10.1127/0935-1221/2013/0025-2280

Caumon, M.-C., Tarantola, A., Mosser-Ruck, R., 2015. Raman spectra of water in fluid inclusions: I. Effect of host mineral birefringence on salinity measurement: Effect of mineral birefringence on salinity measured by Raman spectroscopy. Journal of Raman Spectroscopy 46, 969–976. doi.10.1002/jrs.4708

Cook-Kollars, J., Bebout, G.E., Collins, N.C., Angiboust, S., Agard, P., 2014. Subduction zone metamorphic pathway for deep carbon cycling: I. Evidence from HP/UHP metasedimentary rocks, Italian Alps. Chemical Geology 386, 31–48. doi.10.1016/j.chemgeo.2014.07.013

Dal Piaz, G.V., 1974. Le métamorphisme de haute pression et basse température dans l'évolution structurale du bassin ophiolitique alpino-apenninique. Schweizerische Mineralogische Und Petrographische Mitteilungen 54, 399–424.

Davis, D. W., Lowenstein, T. K., Spencer, R. J., 1990. Melting behavior of fluid inclusions in laboratory-grown halite crystals in the systems NaCl-H2O, NaCl-KCl-H2O, NaCl-MgCl2-H2O, and NaCl-CaCl2-H2O. Geochimica et Cosmochimica Acta, 54, 591-601.

De Wever, P., Caby, R., 1981. Datation de la base des schistes lustrés postophiolitiques par des radiolaires (Oxfordien-Kimmeridgien moyen) dans les Alpes Cottiennes (Saint Véran, France). Comptes Rendus de l'Académie des Sciences de Paris 292, 467–472.

Debret, B., Koga, K.T., Cattani, F., Nicollet, C., Van den Bleeken, G., Schwartz, S., 2016. Volatile (Li, B, F and Cl) mobility during amphibole breakdown in subduction zones. Lithos 244, 165–181. doi.10.1016/j.lithos.2015.12.004

Debret, B., Bouilhol, P., Pons, M.L., Williams, H., 2018. Carbonate Transfer during the Onset of Slab Devolatilization: New Insights from Fe and Zn Stable Isotopes. Journal of Petrology 59, 1145–1166. doi.10.1093/petrology/egy057

Delaney, J.R., Mogk, D.W., Mottl, M., 1987. Quartz-cemented breccias from the Mid-Atlantic Ridge: Samples of a high-salinity hydrothermal upflow zone. Journal of Geophysical Research 92, 9175-9192.

Deville, E., Fudral, S., Lagabrielle, Y., Marthaler, M., Sartori, M., 1992. From oceanic closure to continental collision: A synthesis of the" Schistes lustrés" metamorphic complex of the Western Alps. Geological Society of America Bulletin 104, 127–139.

Diamond, L.W., 2003. Introduction to gas-bearing, aqueous fluid inclusions, in Samson, I., Anderson, A., Marshall, D., 2003. Fluid inclusions: Analysis and Interpretation. Mineral Association of Canada, Short Course 32, 101-158.

Diamond, L.W., Tarantola, A., Stünitz, H., 2010. Modification of fluid inclusions in quartz by deviatoric stress. II: experimentally induced changes in inclusion volume and composition. Contributions to Mineralogy and Petrology 160, 845–864. doi.10.1007/s00410-010-0510-6

Diamond, L.W., Tarantola, A., 2015. Interpretation of fluid inclusions in quartz deformed by weak ductile shearing: Reconstruction of differential stress magnitudes and pre-

deformation fluid properties. Earth and Planetary Science Letters 417, 107-119. doi.10.1016/j.epsl.2015.02.019

Droop, G.T.R., Lombardo, B., Pognante, U., 1990. Formation and distribution of eclogite facies rocks in the Alps, in Carswell, D. A., ed., Eclogite facies rocks: Glasgow, United Kingdom, Blackie, 225-229.

El-Shazly, A.K., Sisson, V.B., 1999. Retrograde evolution of eclogite facies rocks from NE Oman: evidence from fluid inclusions and petrological data. Chemical Geology 154, 193–223. doi.10.1016/S0009-2541(98)00132-6

El-Shazly, A.K., Sisson, V.B., 2004. Fluid inclusions in carpholite-bearing metasediments and blueschists from NE Oman: Constraints on P-T evolution. European Journal of Mineralogy 16, 221–233. doi.10.1127/0935-1221/2004/0016-0221

Endo, S., 2010. Pressure-temperature history of titanite-bearing eclogite from the Western Iratsu body, Sanbagawa Metamorphic Belt, Japan: Titanite eclogite from Sanbagawa Belt. Island Arc 19, 313–335. doi.10.1111/j.1440-1738.2010.00708.x

Epstein, G.S., Bebout, G.E., Angiboust, S., Agard, P., 2020. Scales of fluid-rock interaction and carbon mobility in the deeply underplated and HP-Metamorphosed Schistes Lustrés, Western Alps. Lithos 354–355, 105229. doi.10.1016/j.lithos.2019.105229

Epstein, G.S., Bebout, G.E., Angiboust, S., 2021. Fluid and mass transfer along transient subduction interfaces in a deep paleo-accretionary wedge (Western Alps). Chemical Geology 559, 119920. doi.10.1016/j.chemgeo.2020.119920

Ernst, W. G. (1993). Metamorphism of Franciscan tectonostratigraphic assemblage, Pacheco Pass area, east-central Diablo Range, California coast ranges. Geological Society of America Bulletin 105, 618-636.

Escuder-Viruete, J., Pérez-Estaún, A., 2006. Subduction-related P–T path for eclogites and garnet glaucophanites from the Samaná Peninsula basement complex, northern Hispaniola. International Journal of Earth Sciences (Geol Rundsch) 95, 995–1017. doi.10.1007/s00531-006-0079-5

Fermi, E., 1931. Über den ramaneffekt des kohlendioxyds. Zeitschrift für Physik 71, 250–259.

Fisher, D., Byrne, T., 1990. The character and distribution of mineralized fractures in the Kodiak Formation, Alaska: Implications for fluid flow in an underthrust sequence. Journal of Geophysical Research 95, 9069. doi.10.1029/JB095iB06p09069

Fontaine, F.J., Wilcock, W.S.D., 2006. Dynamics and storage of brine in mid-ocean ridge hydrothermal systems. Journal of Geophysical Research 111. doi.10.1029/2005JB003866

Fontaine, F.J., Wilcock, W.S.D., Butterfield, D.A., 2007. Physical controls on the salinity of mid-ocean ridge hydrothermal vent fluids. Earth and Planetary Science Letters 257, 132–145. doi.10.1016/j.epsl.2007.02.027

Frezzotti, M.L., Selverstone, J., Sharp, Z.D., Compagnoni, R., 2011. Carbonate dissolution during subduction revealed by diamond-bearing rocks from the Alps. Nature Geoscience 4, 703–706. doi.10.1038/ngeo1246

Frezzotti, M.L., Tecce, F., Casagli, A., 2012. Raman spectroscopy for fluid inclusion analysis. Journal of Geochemical Exploration 112, 1–20. doi.10.1016/j.gexplo.2011.09.009

Frezzotti, M.L., Ferrando, S., 2015. The chemical behavior of fluids released during deep subduction based on fluid inclusions. American Mineralogist 100, 352–377. doi.10.2138/am-2015-4933

Frezzotti, M.-L., Huizenga, J.-M., Compagnoni, R., Selverstone, J., 2014. Diamond formation by carbon saturation in C–O–H fluids during cold subduction of oceanic lithosphere. Geochimica et Cosmochimica Acta 143, 68–86. doi.10.1016/j.gca.2013.12.022

Frezzotti, M.L., 2019. Diamond growth from organic compounds in hydrous fluids deep within the Earth. Nature Communications 10, 4952. doi.10.1038/s41467-019-12984-y

Fry, N., Barnicoat, A.C., 1987. The tectonic implications of high-pressure metamorphism in the western Alps. Journal of the Geological Society 144, 653–659. doi.10.1144/gsjgs.144.4.0653

Fudral, S., Deville, E., Marthaler, M., 1987. Distinction de trois ensembles d'unités dans les «Schistes lustrés» compris entre la Vanoise et le Val de Suse (Alpes franco-italiennes septentrionales): aspects lithostratigraphiques, paléogéographiques et géodynamiques.

Comptes rendus de l'Académie des sciences. Série 2, Mécanique, Physique, Chimie, Sciences de l'univers, Sciences de la Terre, 305, 467–472.

Fudral, S., 1996. Etude géologique de la suture tethysienne dans les Alpes franco-italiennes Nord-Occidentales de la Doire Ripaire (Italie) à la région de Bourg Saint-Maurice. PhD thesis Université de Savoie.

Gabalda, S., Beyssac, O., Jolivet, L., Agard, P., Chopin, C., 2009. Thermal structure of a fossil subduction wedge in the Western Alps. Terra Nova 21, 28–34. doi.10.1111/j.1365-3121.2008.00849.x

Gao, J., Klemd, R., Zhang, L., Wang, Z., Xiao, X., 1999. P-T path of high-pressure/low-temperature rocks and tectonic implications in the western Tianshan Mountains, NW China. Journal of Metamorphic Geology 17, 621–636. doi.10.1046/j.1525-1314.1999.00219.x

Gao, J., Klemd, R., 2000. Eclogite occurrences in the Southern Tianshan high-pressure belt, Xinjiang, Western China. Gondwana Research 3, 33-38.

Gao, J., Klemd, R., 2001. Primary fluids entrapped at blueschist to eclogite transition: evidence from the Tianshan meta-subduction complex in northwestern China. Contributions to Mineralogy and Petrology 142, 1-14.

Garber, J.M., Smye, A.J., Feineman, M.D., Kylander-Clark, A.R.C., Matthews, S., 2020. Decoupling of zircon U–Pb and trace-element systematics driven by U diffusion in eclogite-facies zircon (Monviso meta-ophiolite, W. Alps). Contributions to Mineralogy and Petrology 175, 55. doi.10.1007/s00410-020-01692-2

Ghignone, S., Borghi, A., Balestro, G., Castelli, D., Gattiglio, M., Groppo, C., 2020. HP tectono-metamorphic evolution of the Internal Piedmont Zone in Susa Valley (Western Alps): New petrologic insight from garnet+chloritoid-bearing micaschists and Fe–Ti metagabbro. Journal of Metamorphic Geology, 1-26.

Giaramita, M.J., Sorensen, S.S., 1994. Primary fluids in low-temperature eclogites: evidence from two subduction complexes (Dominican Republic, and California, USA). Contributions to Mineralogy and Petrology 117, 279–292. doi.10.1007/BF00310869

Gilio, M., Scambelluri, M., Agostini, S., Godard, M., Pettke, T., Agard, P., Locatelli, M., Angiboust, S., 2020. Fingerprinting and relocating tectonic slices along the plate interface: Evidence from the Lago Superiore unit at Monviso (Western Alps). Lithos 352-353, 105308.

Goffé, B., 1982. Définition du faciès A Fe Mg carpholite-chloritoïde, un marqueur du métamorphisme de HP-BT dans les métasédiments alumineux. PhD thesis Université Pierre et Marie Curie-Paris VI

Goffé, B., Velde, B., 1984. Contrasted metamorphic evolutions in thrusted cover units of the Briançonnais zone (French Alps): a model for the conservation of HP-LT metamorphic mineral assemblages. Earth and Planetary Science Letters 68, 351–360.

Goffé, B., Villey, M., 1984. Texture d'un matériel carboné impliqué dans un métamorphisme haute pression-basse température (Alpes françaises). Les hautes pressions influencent-elles la carbonification ? Bulletin de Minéralogie 107, 81–91. doi.10.3406/bulmi.1984.7795

Goffé, B., Chopin, C., 1986. High-pressure metamorphism in the Western Alps: zoneography of metapelites, chronology and consequences. Schweizerische Mineralogische Und Petrographische Mitteilungen 66, 41–52. doi.10.5169/SEALS-50880

Groppo, C., Beltrando, M., Compagnoni, R., 2009. The P-T path of the ultra-high pressure Lago Di Cignana and adjoining high-pressure meta-ophiolitic units: insights into the evolution of the subducting Tethyan slab. Journal of Metamorphic Geology 27, 207–231. doi.10.1111/j.1525-1314.2009.00814.x

Groppo, C., Rolfo, F., Sachan, H.K., Rai, S.K., 2016. Petrology of blueschist from the Western Himalaya (Ladakh, NW India): Exploring the complex behavior of a lawsonite-bearing system in a paleo-accretionary setting. Lithos 252–253, 41–56. doi.10.1016/j.lithos.2016.02.014

Hacker, B.R., Peacock, S.M., Abers, G.A., Holloway, S.D., 2003. Subduction factory 2. Are intermediate-depth earthquakes in subducting slabs linked to metamorphic dehydration reactions? Journal of Geophysical Research 108. doi.10.1029/2001JB001129

Hacker, B.R., 2008. H$_2$O subduction beyond arcs. Geochemistry Geophysics Geosystems 9. doi.10.1029/2007GC001707

Hall, D.L., Sterner, S.M., 1993. Preferential water loss from synthetic fluid inclusions. Contributions to Mineralogy and Petrology 114, 489–500. doi.10.1007/BF00321753

Handy, M.R., Schmid, S.M., Bousquet, R., Kissling, E., Bernoulli, D., 2010. Reconciling plate-tectonic reconstructions of Alpine Tethys with the geological–geophysical record of spreading and subduction in the Alps. Earth-Science Reviews 102, 121-158.

Hay, W.W., Migdisov, A., Balukhovsky, A.N., Wold, C.N., Flögel, S., Söding, E., 2006. Evaporites and the salinity of the ocean during the Phanerozoic: Implications for climate, ocean circulation and life. Palaeogeography, Palaeoclimatology, Palaeoecology 240, 3–46. doi.10.1016/j.palaeo.2006.03.044

Henry, C., Burkhard, M., Goffé, B., 1996. Evolution of synmetamorphic veins and their wallrocks through a Western Alps transect: no evidence for large-scale fluid flow. Stable isotope, major- and trace-element systematics. Chemical Geology 127, 81–109. doi.10.1016/0009-2541(95)00106-9

Hertwig, A., McClelland, W.C., Kitajima, K., Schertl, H.-P., Maresch, W.V., Stanek, K., Valley, J.W., Sergeev, S.A., 2016. Inherited igneous zircons in jadeitite predate high-pressure metamorphism and jadeitite formation in the Jagua Clara serpentinite mélange of the Rio San Juan Complex (Dominican Republic). Contributions to Mineralogy and Petrology 171, 48. doi.10.1007/s00410-016-1256-6

Holland, T.J.B., 1979. High Water Activities in the Generation of High Pressure Kyanite Eclogites of the Tauern Window, Austria. The Journal of Geology 87, 1–27. doi.10.1086/628388

Huang, F., Daniel, I., Cardon, H., Montagnac, G., Sverjensky, D.A., 2017. Immiscible hydrocarbon fluids in the deep carbon cycle. Nature Communications 8, 15798. doi.10.1038/ncomms15798

Hyndman, R.D., McCrory, P.A., Wech, A., Kao, H., Ague, J., 2015. Cascadia subducting plate fluids channelled to fore-arc mantle corner: ETS and silica deposition. Journal of Geophysical Research: Solid Earth 120, 4344–4358. doi.10.1002/2015JB011920

Inglis, E.C., Debret, B., Burton, K.W., Millet, M.-A., Pons, M.-L., Dale, C.W., Bouilhol, P., Cooper, M., Nowell, G.M., McCoy-West, A.J., Williams, H.M., 2017. The behavior of iron and zinc stable isotopes accompanying the subduction of mafic oceanic crust: A case study from Western Alpine ophiolites. Geochemistry Geophysics Geosystems 18, 2562–2579. doi.10.1002/2016GC006735

Invernizzi, C., Bigazzi, G., Corrado, S., Leo, P.D., Schiattarella, M., Zattin, M., 2008 New thermobaric constraints on the exhumation history of the Liguride accretionary wedge, southern Italy. Ofioliti 33, 21-32.

Laurent, V., Lanari, P., Naïr, I., Augier, R., Lahfid, A., Jolivet, L., 2018. Exhumation of eclogite and blueschist (Cyclades, Greece): Pressure-temperature evolution determined by thermobarometry and garnet equilibrium modelling. Journal of Metamorphic Geology 36, 769-798.

Ito, E., Anderson, A.T., 1983. Submarine metamorphism of gabbros from the Mid-Cayman Rise: Petrographic and mineralogic constraints on hydrothermal processes at slow-spreading ridges. Contributions to Mineralogy and Petrology 82, 371–388. doi.10.1007/BF00399714

Jaeckel, K., Bebout, G.E., Angiboust, S., 2018. Deformation-enhanced fluid and mass transfer along Western and Central Alps paleo-subduction interfaces: Significance for carbon cycling models. Geosphere 14, 2355–2375. doi.10.1130/GES01587.1

Jamieson, R.A., Craw, D., 1987. Sphalerite geobarometry in metamorphic terranes: an appraisal with implications for metamorphic pressure in the Otago Schist. Journal of Metamorphic Geology 5, 87–99. doi.10.1111/j.1525-1314.1987.tb00371.x

Kawamoto, T., Hertwig, A., Shertl, H.-P., Maresch, W.V., 2018. Fluid inclusions in jadeitite and jadeite-rich rock from serpentinite mélanges in northern Hispaniola: Trapped ambient fluids in a cold subduction channel. Lithos 308-309, 227-241.

Kelley, D.S., Delaney, J.R., 1987. Two-phase separation and fracturing in mid-ocean ridge gabbros at temperatures greater than 700°C. Earth and Planetary Science Letters 83, 53–66. doi.10.1016/0012-821X(87)90050-1

Kelley, D.S., Robinson, P.T., Malpas, J.G., 1992. Processes of brine generation and circulation in the oceanic crust: Fluid inclusion evidence from the Troodos Ophiolite, Cyprus. Journal of Geophysical Research 97, 9307. doi.10.1029/92JB00520

Klemd, R., Van den Kerkhof, A.M., Horn, E.E., 1992. High-density CO_2-N_2 inclusions in eclogite-facies metasediments of the Mfinchberg gneiss complex, SE Germany. Contributions to Mineralogy and Petrology 111, 409–419.

Kolesnikov, A., Kutcherov, V.G., Goncharov, A.F., 2009. Methane-derived hydrocarbons produced under upper-mantle conditions. Nature Geoscience 2, 566–570. doi.10.1038/ngeo591

Küster, M., Stöckhert, B., 1997. Density changes of fluid inclusions in high-pressure low-temperature metamorphic rocks from Crete: A thermobarometric approach based on the creep strength of the host minerals. Lithos 41, 151–167. doi.10.1016/S0024-4937(97)82010-5

Lafay, R., Deschamps, F., Schwartz, S., Guillot, S., Godard, M., Debret, B., Nicollet, C., 2013. High-pressure serpentinites, a trap-and-release system controlled by metamorphic conditions: Example from the Piedmont zone of the western Alps. Chemical Geology 343, 38–54. doi.10.1016/j.chemgeo.2013.02.008

Lagabrielle, Y., 1987. Les ophiolites : Marqueurs de l'histoire tectonique des domaines océaniques. PhD thesis Brest.

Lagabrielle, Y., Cannat, M., 1990. Alpine Jurassic ophiolites resemble the modern central Atlantic basement. Geology 18, 319–322.

Lagabrielle, Y., Vitale Brovarone, A., Ildefonse, B., 2015. Fossil oceanic core complexes recognized in the blueschist metaophiolites of Western Alps and Corsica. Earth-Science Reviews 141, 1–26. doi.10.1016/j.earscirev.2014.11.004

Lapen, T.J., Johnson, C.M., Baumgartner, L.P., Mahlen, N.J., Beard, B.L., Amato, J.M., 2003. Burial rates during prograde metamorphism of an ultra-high-pressure terrane: an example from Lago di Cignana, western Alps, Italy. Earth and Planetary Science Letters 215, 57–72. doi.10.1016/S0012-821X(03)00455-2

Le, V.-H., Caumon, M.-C., Tarantola, A., Randi, A., Robert, P., Mullis, J., 2019. Quantitative Measurements of Composition, Pressure, and Density of Microvolumes of CO_2–N_2 Gas Mixtures by Raman Spectroscopy. Analytical Chemistry 91, 14359–14367. doi.10.1021/acs.analchem.9b02803

Le, V.-H., Caumon, M.-C., Tarantola, A., Randi, A., Robert, P., Mullis, J., 2020. Calibration data for simultaneous determination of P-V-X properties of binary and ternary CO2 - CH4 - N2 gas mixtures by Raman spectroscopy over 5–600 bar: Application to natural fluid inclusions. Chemical Geology 552, 119783. doi.10.1016/j.chemgeo.2020.119783

Le Pichon, X., Bergerat, F., Roulet, M., 1988. Plate kinematics and tectonics leading to the Alpine belt formation: a new analysis. Geological Society of America Special Issue 218, 111–131.

Lefeuvre, B., Agard, P., Verlaguet, A., Dubacq, B., Plunder, A., 2020. Massive formation of lawsonite in subducted sediments from the Schistes Lustrés (W. Alps): Implications for mass transfer and decarbonation in cold subduction zones. Lithos 370–371, 105629. doi.10.1016/j.lithos.2020.105629

Lefeuvre, B., 2020. La lawsonite dans les métasédiments en base de zone sismogénique : géochimie, échelles de migration des fluides et rôle de la déformation dans les Schistes Lustrés. PhD thesis, Sorbonne Université Paris.

Lemoine, M., Marthaler, M., Caron, M., Sartori, M., Amaudric du Chaffaut, S., 1984. Découverte de foraminifères planctoniques du Crétacé supérieur dans les schistes lustrés du Queyras (Alpes occidentales). Conséquences paléogéographiques et tectoniques. Comptes-rendus des séances de l'Académie des sciences. Série 2, Mécanique-physique, chimie, sciences de l'univers, sciences de la terre 299, 727–732.

Lemoine, M., Tricart, P., 1986. Les Schistes lustrés piémontais des Alpes Occidentales : approche stratigraphique, structurales et sédimentologique. Eclogae Geologicae Helvetiae 79, 271–294. doi.10.5169/SEALS-165835

Li, Y., 2017. Immiscible C-H-O fluids formed at subduction zone conditions. Geochemichal Perspectives Letters 3, 12–21. doi.10.7185/geochemlet.1702

Locatelli, M., Verlaguet, A., Agard, P., Federico, L., Angiboust, S., 2018. Intermediate-depth brecciation along the subduction plate interface (Monviso eclogite, W. Alps). Lithos 320–321, 378–402. doi.10.1016/j.lithos.2018.09.028

Locatelli, M., Federico, L., Agard, P., Verlaguet, A., 2019a. Geology of the southern Monviso metaophiolite complex (W-Alps, Italy). Journal of Maps 15, 283–297. doi.10.1080/17445647.2019.1592030

Locatelli, M., Verlaguet, A., Agard, P., Pettke, T., Federico, L., 2019b. Fluid Pulses During Stepwise Brecciation at Intermediate Subduction Depths (Monviso Eclogites, W. Alps): First Internally Then Externally Sourced. Geochemistry Geophysics Geosystems 20, 5285–5318. doi.10.1029/2019GC008549

Lombardo, B., 1978. Osservazioni preliminari sulle ofioliti metamorfiche del Monviso (Alpi Occidentali). Rendiconti Della Soc. Ital. Mineral. E Petrol. 34, 235–305.

Luckscheiter, B., Morteani, G., 1980. The fluid phase in eclogites, glaucophane-bearing rocks and amphibolites from the central tauern window as deduced from fluid inclusion studies. TMPM Tschermaks Petr. Mitt. 27, 99–111. doi.10.1007/bf01082401

Mangenot, X., Tarantola, A., Mullis, J., Girard, J.P., Le, V.H., Eiler, J.M., 2021. Geochemistry of clumped isotopologues of CH4 within fluid inclusions in Alpine tectonic quartz fissures. Earth and Planetary Science Letters 561, 116792

McCollom, T.M., 2013. Laboratory Simulations of Abiotic Hydrocarbon Formation in Earth's Deep Subsurface. Reviews in Mineralogy and Geochemistry 75, 467–494. doi.10.2138/rmg.2013.75.15

Meneghini, F., Marroni, M., Moore, J.C., Pandolfi, L., Rowe, C.D., 2009. The processes of underthrusting and underplating in the geologic record: structural diversity between the Franciscan Complex (California), the Kodiak Complex (Alaska) and the Internal Ligurian Units (Italy). Geological Journal 44, 126–152. doi.10.1002/gj.1144

Messiga, B., Scambelluri, M., Piccardo, G.B., 1995. Chloritoid-bearing assemblages in mafic systems and eclogite-facies hydration of alpine Mg-Al metagabbros (Erro-Tobbio Unit, Ligurian Western Alps). European Journal of Mineralogy 7, 1149–1168. doi.10.1127/ejm/7/5/1149

Michard, A., Goffé, B., Chopin, C., Henry, C., 1996. Did the Western Alps develop through an Oman-type stage? The geotectonic setting of high-pressure metamorphism in two contrasting Tethyan transects. Eclogae Geologicae Helvetiae 89, 43–80.

Monaco, C., Tortorici, L., 1995. Tectonic role of ophiolite-bearing terranes in the development of the Southern Apennines orogenic belt. Terra Nova 7, 153–160. doi.10.1111/j.1365-3121.1995.tb00684.x

Mukherjee, B.K., Sachan, H.K., 2009. Fluids in coesite-bearing rocks of the Tso Morari Complex, NW Himalaya: evidence for entrapment during peak metamorphism and subsequent uplift. Geological Magazine 146, 876–889. doi.10.1017/S0016756809990069

Mullis, J., 1979. The system methane-water as a geologic thermometer and barometer from the external part of the Central Alps. Bulletin de Minéralogie 102, 526–536. doi.10.3406/bulmi.1979.7301

Mullis, J., Dubessy, J., Poty, B., O'Neil, J., 1994. Fluid regimes during late stages of a continental collision: Physical, chemical, and stable isotope measurements of fluid inclusions in fissure quartz from a geotraverse through the Central Alps, Switzerland. Geochimica et Cosmochimica Acta 58, 2239–2267. doi.10.1016/0016-7037(94)90008-6

Muñoz-Montecinos, J., Angiboust, S., Cambeses, A., García-Casco, A., 2020. Multiple veining in a paleo–accretionary wedge: The metamorphic rock record of prograde dehydration and transient high pore-fluid pressures along the subduction interface (Western Series, central Chile). Geosphere 16, 765–786. doi.10.1130/GES02227.1

Nadeau, S., Philippot, P., Pineau, F., 1993. Fluid inclusion and mineral isotopic compositions (HCO) in eclogitic rocks as tracers of local fluid migration during high-pressure metamorphism. Earth and Planetary Science Letters 114, 431–448. doi.10.1016/0012-821X(93)90074-J

Nehlig, P., 1991. Salinity of oceanic hydrothermal fluids: a fluid inclusion study. Earth and Planetary Science Letters 102, 310–325. doi.10.1016/0012-821X(91)90026-E

Obara, K., 2002. Nonvolcanic Deep Tremor Associated with Subduction in Southwest Japan. Science 296, 1679–1681. doi.10.1126/science.1070378

Padrón-Navarta, J.A., Hermann, J., Garrido, C.J., López Sánchez-Vizcaíno, V., Gómez-Pugnaire, M.T., 2010. An experimental investigation of antigorite dehydration in natural silica-enriched serpentinite. Contributions to Mineralogy Petrology 159, 25–42. doi.10.1007/s00410-009-0414-5

Philippot, P., 1987. "Crack seal" vein geometry in eclogitic rocks. Geodinamica Acta 1, 171–181.

Philippot, P., Kienast, J.-R., 1989. Chemical-microstructural changes in eclogite-facies shear zones (Monviso, Western Alps, north Italy) as indicators of strain history and the mechanism and scale of mass transfer. Lithos 23, 179–200. doi.10.1016/0024-4937(89)90004-2

Philippot, P., 1990. Opposite vergence of Nappes and crustal extension in the French-Italian western Alps. Tectonics 9, 1143–1164. doi.10.1029/TC009i005p01143

Philippot, P., Selverstone, J., 1991. Trace-element-rich brines in eclogitic veins: implications for fluid composition and transport during subduction. Contributions to Mineralogy and Petrology 106, 417–430. doi.10.1007/BF00321985

Philippot, P., Agrinier, P., Scambelluri, M., 1998. Chlorine cycling during subduction of altered oceanic crust. Earth and Planetary Science Letters 12.

Plunder, A., Agard, P., Dubacq, B., Chopin, C., Bellanger, M., 2012. How continuous and precise is the record of P-T paths? Insights from combined thermobarometry and thermodynamic modelling into subduction dynamics (Schistes Lustrés, W. Alps). Journal of Metamorphic Geology 30, 323–346. doi.10.1111/j.1525-1314.2011.00969.x

Pognante, U., 1991. Petrological constraints on the eclogite- and blueschist facies metamorphism and P-T-t paths in the Western Alps. Journal of Metamorphic Geology 9, 5–17. doi.10.1111/j.1525-1314.1991.tb00501.x

Pourteau, A., Bousquet, R., Vidal, O., Plunder, A., Duesterhoeft, E., Candan, O., & Oberhänsli, R. (2014). Multistage growth of Fe–Mg–carpholite and Fe–Mg–chloritoid, from field evidence to thermodynamic modelling. Contributions to Mineralogy and Petrology, 168, 1090.

Raimbourg, H., Thiéry, R., Vacelet, M., Ramboz, C., Cluzel, N., Le Trong, E., Yamaguchi, A., Kimura, G., 2014. A new method of reconstituting the P–T conditions of fluid circulation in an accretionary prism (Shimanto, Japan) from microthermometry of methane-bearing aqueous inclusions. Geochimica et Cosmochimica Acta 125, 96–109. doi.10.1016/j.gca.2013.09.025

Raimbourg, H., Vacelet, M., Ramboz, C., Famin, V., Augier, R., Palazzin, G., Yamaguchi, A., Kimura, G., 2015. Fluid circulation in the depths of accretionary prisms: an example of the Shimanto Belt, Kyushu, Japan. Tectonophysics 655, 161–176. doi.10.1016/j.tecto.2015.05.023

Raimbourg, H., Famin, V., Palazzin, G., Mayoux, M., Jolivet, L., Ramboz, C., Yamaguchi, A., 2018. Fluid properties and dynamics along the seismogenic plate interface. Geosphere 14, 469–491. doi.10.1130/GES01504.1

Roedder, E. (1984). Fluid Inclusions. Reviews in Mineralogy, Vol. 12, Mineralogical Society of America, 644 p.

Rossetti, F., Tecce, F., Aldega, L., Brilli, M., Faccenna, C., 2006. Deformation and fluid flow during orogeny at the palaeo-Pacific active margin of Gondwana: The Early Palaeozoic Robertson Bay accretionary complex (north Victoria Land, Antarctica). Journal of Metamorphic Geology 24, 33–53. doi.10.1111/j.1525-1314.2005.00620.x

Rubatto, D., Hermann, J., 2003. Zircon formation during fluid circulation in eclogites (Monviso, Western Alps): implications for Zr and Hf budget in subduction zones. Geochimica et Cosmochimica Acta 67, 2173–2187.

Rubatto, D., Angiboust, S., 2015. Oxygen isotope record of oceanic and high-pressure metasomatism: a P–T–time–fluid path for the Monviso eclogites (Italy). Contributions to Mineralogy and Petrology 170, 44. doi.10.1007/s00410-015-1198-4

Rupke, L., Morgan, J, Hort, M, Connolly, J, 2004. Serpentine and the subduction zone water cycle. Earth and Planetary Science Letters 223, 17–34. doi.10.1016/j.epsl.2004.04.018

Sachan, H.K., Kharya, A., Singh, P.C., Rolfo, F., Groppo, C., Tiwari, S.K., 2017. A fluid inclusion study of blueschist-facies lithologies from the Indus suture zone, Ladakh (India): Implications for the exhumation of the subduction related Sapi-Shergol ophiolitic mélange. Journal of Asian Earth Sciences 146, 185–195. doi.10.1016/j.jseaes.2017.05.025

Sadofsky, S.J., Bebout, G.E., 2004. Field and Isotopic Evidence for Fluid Mobility in the Franciscan Complex: Forearc Paleohydrogeology to Depths of 30 Kilometers. International Geology Review 46, 1053–1088. doi.10.2747/0020-6814.46.12.1053

Saliot, P., 1979. La jadéite dans les Alpes françaises. Bulletin de Minéralogie 102, 391–401. doi.10.3406/bulmi.1979.7335

Scambelluri, M., Piccardo, G., Philippot, P., Robbiano, A., Negretti, L., 1997. High salinity fluid inclusions formed from recycled seawater in deeply subducted alpine serpentinite. Earth and Planetary Science Letters 148, 485–499. doi.10.1016/S0012-821X(97)00043-5

Scambelluri, M., Pennacchioni, G., Philippot, P., 1998. Salt-rich aqueous fluids formed during eclogitization of metabasites in the Alpine continental crust (Austroalpine Mt. Emilius unit, Italian western Alps). Lithos 43, 151–167.

Scambelluri, M., Bottazzi, P., Trommsdorff, V., Vannucci, R., Hermann, J., Gomez-Pugnaire, M.T., Lopez-Sanchez, V., 2001. Incompatible element-rich fluids released by antigorite breakdown in deeply subducted mantle. Earth and Planetary Science Letters 192, 457-470.

Scambelluri, M., Philippot, P., 2001. Deep fluids in subduction zones. Lithos 55, 213–227. doi.10.1016/S0024-4937(00)00046-3

Schertl, H.-P., Maresch, W.V., Stanek, K. P., Hertwig, A., Krebs, M., Baese, R., Sergeev, S.S., 2012. New occurrences of jadeitite, jadeite quartzite and jadeite-lawsonite quartzite in the Dominican Republic, Hispaniola: petrological and geochronological overview. European Journal of Mineralogy 24, 199–216. doi.10.1127/0935-1221/2012/0024-2201

Schmid, S.M., Pfiffner, O.A., Froitzheim, N., Schönborn, G., Kissling, E., 1996. Geophysical-geological transect and tectonic evolution of the Swiss-Italian Alps. Tectonics 15, 1036–1064. doi.10.1029/96TC00433

Schmid, S.M., Kissling, E., Diehl, T., van Hinsbergen, D.J.J., Molli, G., 2017. Ivrea mantle wedge, arc of the Western Alps, and kinematic evolution of the Alps–Apennines orogenic system. Swiss Journal of Geosciences 110, 581–612. doi.10.1007/s00015-016-0237-0

Schmidt, M.W., Poli, S., 2014. Devolatilization During Subduction, in: Treatise on Geochemistry. Elsevier, pp. 669–701. doi.10.1016/B978-0-08-095975-7.00321-1

Schwartz, S., 2000. La zone piémontaise des Alpes Occidentales : un paléocomplexe de subduction. Arguments métamorphiques, géochronologiques et structuraux. PhD thesis Université Claude Bernard-Lyon I.

Schwartz, S., Lardeaux, J.-M., Guillot, S., Tricart, P., 2000. Diversité du métamorphisme éclogitique dans le massif ophiolitique du Monviso (Alpes occidentales, Italie). Geodinamica Acta 13, 169–188. doi.10.1080/09853111.2000.11105371

Schwartz, S., Lardeaux, J.M., Tricart, P., Guillot, S., Labrin, E., 2007. Diachronous exhumation of HP-LT metamorphic rocks from south-western Alps: evidence from fission-track analysis. Terra Nova 19, 133–140. doi.10.1111/j.1365-3121.2006.00728.x

Schwartz, S., Guillot, S., Reynard, B., Lafay, R., Debret, B., Nicollet, C., Lanari, P., Auzende, A.L., 2013. Pressure–temperature estimates of the lizardite/antigorite transition in high pressure serpentinites. Lithos 178, 197–210. doi.10.1016/j.lithos.2012.11.023

Schwartz, S., Gautheron, C., Ketcham, R.A., Brunet, F., Corre, M., Agranier, A., Pinna-Jamme, R., Haurine, F., Monvoin, G., Riel, N., 2020. Unraveling the exhumation history of high-

pressure ophiolites using magnetite (U-Th-Sm)/He thermochronometry. Earth and Planetary Science Letters 543, 116359. doi.10.1016/j.epsl.2020.116359

Selverstone, J., Franz, G., Thomas, S., Getty, S., 1992. Fluid variability in 2 GPa eclogites as an indicator of fluid behavior during subduction. Contributions to Mineralogy and Petrology 112, 341–357. doi.10.1007/BF00310465

Selverstone, J., Sharp, Z.D., 2013. Chlorine isotope constraints on fluid-rock interactions during subduction and exhumation of the Zermatt-Saas ophiolite. Geochemistry Geophysics Geosystems 14, 4370–4391. doi.10.1002/ggge.20269

Sicard-Lochon, E., 1987. La lawsonite et ses pseudomorphoses. PhD thesis Université Claude Bernard-Lyon I.

Sisson, V.B., Hollister, L.S., Onstott, T.C., 1989. Petrologic and age constraints on the origin of a low-pressure/high-temperature metamorphic complex, southern Alaska. Journal of Geophysical Research 94, 4392–4410. doi.10.1029/JB094iB04p04392

Smith, M.P., Yardley, B.W.D., 1999. Fluid evolution during metamorphism of the Otago Schist, New Zealand: (I) Evidence from fluid inclusions. Journal of Metamorphic Geology 17, 173–186. doi.10.1046/j.1525-1314.1999.00189.x

Spandler, C., Pettke, T., Rubatto, D., 2011. Internal and External Fluid Sources for Eclogite-facies Veins in the Monviso Meta-ophiolite, Western Alps: Implications for Fluid Flow in Subduction Zones. Journal of Petrology 52, 1207–1236. doi.10.1093/petrology/egr025

Spandler, C., Pirard, C., 2013. Element recycling from subducting slabs to arc crust: A review. Lithos 170–171, 208–223. doi.10.1016/j.lithos.2013.02.016

Spear, F.S., Franz, G., 1986. P-T evolution of metasediments from the Eclogite Zone, south-central Tauern Window, Austria. Lithos 19, 219–234. doi.10.1016/0024-4937(86)90024-1

Stampfli, G.M., Mosar, J., Marquer, D., Marchant, R., Baudin, T., Borel, G., 1998. Subduction and obduction processes in the Swiss Alps. Tectonophysics 296, 159–204. doi.10.1016/S0040-1951(98)00142-5

Starr, P.G., Broadwell, K.S., Dragovic, B., Scambelluri, M., Haws, A.A., Caddick, M,J., Smye, A,J., Baxter, E,F., 2020. The subduction and exhumation history of the Voltri Ophiolite, Italy: Evaluating exhumation mechanisms for high-pressure metamorphic massifs. Lithos 376-377, 105767.

Sterin, K.E., Aleksanyan, V.T., Zhizhin, G.N., 1980. Raman spectra of hydrocarbons, Pergamon. ed.

Sterner, S.M., Bodnar, R.J., 1989. Synthetic fluid inclusions - VII. Re-equilibration of fluid inclusions in quartz during laboratory-simulated metamorphic burial and uplift. Journal of Metamorphic Geology 7, 243–260. doi.10.1111/j.1525-1314.1989.tb00587.x

Sverjensky, D., Daniel, I., Brovarone, A.V., 2020. The Changing Character of Carbon in Fluids with Pressure: Organic Geochemistry of Earth's Upper Mantle Fluids, in: Manning, C.E., Lin, J., Mao, W.L. (Eds.), Geophysical Monograph Series. Wiley, pp. 259–269. doi.10.1002/9781119508229.ch22

Tao, R., Zhang, L., Tian, M., Zhu, J., Liu, X., Liu, J., Höfer, H.E., Stagno, V., Fei, Y., 2018. Formation of abiotic hydrocarbon from reduction of carbonate in subduction zones: Constraints from petrological observation and experimental simulation. Geochimica et Cosmochimica Acta 239, 390–408. doi.10.1016/j.gca.2018.08.008

Tarantola, A., Mullis, J., Vennemann, T., Dubessy, J., de Capitani, C., 2007. Oxidation of methane at the CH4/H2O–(CO2) transition zone in the external part of the Central Alps, Switzerland: Evidence from stable isotope investigations. Chemical Geology 237, 329–357. doi.10.1016/j.chemgeo.2006.07.007

Tarantola, A., Mullis, J., Guillaume, D., Dubessy, J., de Capitani, C., Abdelmoula, M., 2009. Oxidation of CH4 to CO2 and H2O by chloritization of detrital biotite at 270±5 °C in the external part of the Central Alps, Switzerland. Lithos 112, 497–510. doi.10.1016/j.lithos.2009.04.008

Tarantola, A., Diamond, L.W., Stünitz, H., Thust, A., Pec, M., 2012. Modification of fluid inclusions in quartz by deviatoric stress. III: Influence of principal stresses on inclusion density and orientation. Contributions to Mineralogy and Petrology 164, 537–550. doi.10.1007/s00410-012-0749-1

Tarantola, A., Caumon, M.-C., 2015. Raman spectra of water in fluid inclusions: II. Effect of negative pressure on salinity measurement: Effect of negative pressure on salinity measured by Raman spectroscopy. Journal of Raman Spectroscopy 46, 977–982. doi.10.1002/jrs.4668

Terabayashi, M., Maruyama, S., 1998. Large pressure gap between the Coastal and Central Franciscan belts, northern and central California. Tectonophysics 285, 87–101. doi.10.1016/S0040-1951(97)00194-7

Toriumi, M., and J. Teruya (1988), Tectono-metamorphism of the Shimanto Belt, Mod. Geol. 12, 303–324.

Touret, J.L.R., Frezzotti, M.-L., 2003. Fluid inclusions in high pressure and ultrahigh pressure metamorphic rocks, in: Papp, G., Weiszburg, T.G., Carswell, D.A., Compagnoni, R., Rolfo, F. (Eds.), Ultrahigh Pressure Metamorphism. Mineralogical Society of Great Britain and Ireland, Budapest, pp. 467–487. doi.10.1180/EMU-notes.5.15

Tricart, P., Schwartz, S., 2006. A north-south section across the Queyras Schistes lustrés (Piedmont zone, Western Alps): Syn-collision refolding of a subduction wedge. Eclogae Geologicae Helvetiae 99, 429–442. doi.10.1007/s00015-006-1197-6

Tsujimori, T., Matsumoto, K., Wakabayashi, J., Liou, J.G., 2006. Franciscan eclogite revisited: Reevaluation of the P–T evolution of tectonic blocks from Tiburon Peninsula, California, U.S.A. Mineralogy and Petrology 88, 243–267. doi.10.1007/s00710-006-0157-1

Vallis, F., Scambelluri, M., 1996. Redistribution of high-pressure fluids during retrograde metamorphism of eclogite-facies rocks (Voltri Massif, Italian Western Alps). Lithos 39, 81–92. doi.10.1016/S0024-4937(96)00012-6

Vanko, D. A., 1986. High-chlorine amphiboles from oceanic rocks: product of highly-saline hydrothermal fluids? American Mineralogist 71, 51-59.

Vanko, D.A., 1988 Temperature, pressure, and composition of hydrothermal fluids, with their bearing on the magnitude of tectonic uplift at mid-ocean ridges, inferred from fluid inclusions in oceanic layer 3 rocks. Journal of Geophysical Research 93, 4595-4611.

Vannucchi, P., 2001. Monitoring paleo-fluid pressure through vein microstructures. Journal of Geodynamics 32, 567–581. doi.10.1016/S0264-3707(01)00048-5

Verlaguet, A., Bonnemains, D., Mével, C., Escartín, J., Andreani, M., Bourdelle, F., Boiron, M. -C., Chavagnac, V., 2020. Fluid circulation along an oceanic detachment fault: insights from fluid inclusions in silicified brecciated fault rocks (Mid-Atlantic Ridge at 13°20'N). Geochemistry Geophysics Geosystems. doi.10.1029/2020GC009235

Vitale Brovarone, A., Alard, O., Beyssac, O., Martin, L., Picatto, M., 2014. Lawsonite metasomatism and trace element recycling in subduction zones. Journal of Metamorphic Geology 32, 489–514. doi.10.1111/jmg.12074

Vitale Brovarone, A., Martinez, I., Elmaleh, A., Compagnoni, R., Chaduteau, C., Ferraris, C., Esteve, I., 2017. Massive production of abiotic methane during subduction evidenced in metamorphosed ophicarbonates from the Italian Alps. Nature Communications 8, 14134. doi.10.1038/ncomms14134

Vitale Brovarone, A., Sverjensky, D.A., Piccoli, F., Ressico, F., Giovannelli, D., Daniel, I., 2020a. Subduction hides high-pressure sources of energy that may feed the deep subsurface biosphere. Nature Communications 11, 3880. doi.10.1038/s41467-020-17342-x

Vitale Brovarone, A., Tumiati, S., Piccoli, F., Ague, J.J., Connolly, J.A.D., Beyssac, O., 2020b. Fluid-mediated selective dissolution of subducting carbonaceous material: Implications for carbon recycling and fluid fluxes at forearc depths. Chemical Geology 549, 119682. doi.10.1016/j.chemgeo.2020.119682

Vityk, M.O., Bodnar, R.J., 1995a. Do fluid inclusions in high-grade metamorphic terranes preserve peak metamorphic density during retrograde decompression? American Mineralogist 80, 641–644.

Vityk, M.O., Bodnar, R.J., 1995b. Textural evolution of synthetic fluid inclusions in quartz during reequilibration, with applications to tectonic reconstruction. Contributions to Mineralogy and Petrology 121, 309–323. doi.10.1007/BF02688246

Vrolijk, P., 1987. Tectonically driven fluid flow in the Kodiak accretionary complex, Alaska. Geology 15, 466–469.

Vrolijk, P., Myers, G., Moore, J.C., 1988. Warm fluid migration along tectonic melanges in the Kodiak Accretionary Complex, Alaska. Journal of Geophysical Research 93, 10313–10324. doi.10.1029/JB093iB09p10313

Widmer, T., Thompson, A.B., 2001. Local origin of high pressure vein material in eclogite facies rocks of the Zermatt-Saas-Zone, Switzerland. American Journal of Science 301, 627–656. doi.10.2475/ajs.301.7.627

Yardley, B.W.D., 1982. The early metamorphic history of the Haast Schists and related rocks of New Zealand. Contributions to Mineralogy and Petrology 81, 317–327. doi.10.1007/BF00371686

Yardley, B.W.D., Graham, J.T., 2002. The origins of salinity in metamorphic fluids: Origins of salinity in metamorphic fluids. Geofluids 2, 249–256. doi.10.1046/j.1468-8123.2002.00042.x

Yoshida, K., Hirajima, T., Ohsawa, S., Kobayashi, T., Mishima, T., Sengen, Y., 2015. Geochemical features and relative B–Li–Cl compositions of deep-origin fluids trapped in high-pressure metamorphic rocks. Lithos 226, 50–64. doi.10.1016/j.lithos.2015.03.002

Wopenka, B., Pasteris, J.D., 1987. Raman intensities and detection limits of geochemically relevant gas mixtures for a laser Raman microprobe. Analytical Chemistry 59, 2165-2170.

Figure 1: Compilation of exhumed oceanic subduction rocks for which primary FI were analyzed in the literature, placed on a schematic subduction zone according to their estimated burial depth. The scope of this study is represented by red-border rectangles. References for studies of both fluid inclusions and P-T estimates are reported in Table 1. The size of the circles corresponds to the number of salinity values from primary FI available for each oceanic subduction compiled in Table 1. The lower bound of the smallest circle corresponds to 0 or unspecified in the corresponding studies.

Figure 2: Map and cross-section of the studied area. A) Simplified geological map of the Western Alps with focus on the Schistes Lustrés complex and the distribution of metamorphic facies within. The studied area is outlined by the black dashed square. DB: Dent Blanche; MR: Monte Rosa; GP: Gran Paradiso; DM: Dora Maira; Brianç: Briançonnais; Che.: Chenaillet. B) Simplified geological map of the studied area with distribution of tectonometamorphic units after Lagabrielle (1987). Studied outcrops are localized by stars and described in Table 2. C) Schematic cross-section of the studied traverse and eastward-increasing gradient of peak metamorphic conditions (modified after Lagabrielle, 1987) with P-T estimates from Agard et al. (2001), Schwartz et al. (2013) and Angiboust et al. (2012b).

Figure 3: Metamorphic evolution of the Schistes Lustrés complex units. P-T estimates are from Agard et al. (2001), Schwartz et al. (2013) and Angiboust et al. (2012b). Lawsonite and carpholite stability fields for metasediments are reported from Lefeuvre et al. (2020), Bebout et al. (2013) and Pourteau et al. (2014). Garnet-omphacite stability field for metamafic rocks is after Angiboust and Agard (2010). Fluid release associated with carpholite or lawsonite breakdown, or garnet formation, is indicative and corresponds to generalized P-T conditions. Lws: lawsonite; Car: carpholite; Jd: jadeite; Qz: quartz; Ab: albite.

Figure 4: Field observations. A) Metapelitic outcrop from LPU1 exposing a huge density of veins. B), C) Quartz-lawsonite-ankerite vein showing elongated creamy-coloured LwsB crystals parallel to vein walls. D) Small tensile LwsC vein with ankerite and quartz. E) Closer-view of C sample exposing the association of LwsB fibers with ankerite and quartz. F) Close-up view of LwsC 'en échelon' veins illustrating the association of LwsC with quartz and ankerite. G) Metagabbroic blueschist-facies block from LPU1 containing few veins of greenish-jadeite. H) Close view of omphacite-bearing veins crosscutting an eclogite-facies

garnet-rich metagabbro from LPL. Lws: lawsonite; Ank: ankerite; Qz: quartz; Gln: glaucophane.

Figure 5: Microphotographs of veins illustrating mineral crystallization textures and trapped primary fluid inclusions. A) Thick-section of LwsB-bearing vein from LPU1. B) Closer-view of A) showing textural equilibrium between lawsonite (Lws) and quartz (Qz) fibers. C) Closer-view of B) showing isolated primary fluid inclusions in the quartz co-crystallizing with lawsonite. D) Thick section of carpholite (Car)-bearing vein sample from LPU1. E) Closer-view of D) exposing quartz full of carpholite needles. F) Closer-view of E) showing an isolated primary fluid inclusion in quartz co-crystallizing with carpholite.

Figure 6: Raman spectra of the liquid phase of three fluid different inclusions in quartz of LwsB-bearing veins and in omphacite from eclogitic breccia matrices. The variable shape of the chlorinity band allows calculation of salinity following the method of Caumon et al. (2013). a.u.: arbitrary unit.

Figure 7: Salinity estimated by microthermometry versus salinity estimated by Raman spectroscopy in the same inclusions. Taking into account the respective uncertainties of these methods (0.2 wt% NaCl eq. for microthermometry and 0.4 wt% NaCl eq. for Raman considering the methodology of Caumon et al., 2013) all points are crossing the 1:1 line showing the validity and accuracy of Caumon et al. (2013) method in our samples.

Figure 8: Raman spectra of the main gases identified FI vapor bubbles. a) CO_2 presence was detected by identification of the Fermi diad (Fermi, 1931; 1285 and 1388 cm^{-1} peaks) and CH_4 by appearance of the 2917 cm^{-1} peak (Frezzotti et al., 2012). b) N_2 is characterized by a peak at 2331 cm^{-1} (Frezzotti et al., 2012) and calculated by substraction of atmospherical N_2 peak area (outside the FI) a.u.: arbitrary unit.

Figure 9: Microphotographs of fluid inclusions. A) FI-rich quartz (Qz) showing textural equilibrium with LwsB fibers. B) and C) Biphase (liquid L + vapor V) well-defined inclusions in quartz from lawsonite (Lws)-bearing veins. D) Biphase (L+V) fluid inclusion with irregular shape, in quartz from a lawsonite-bearing vein. E) Rare triphase (L+V+ solid S) fluid inclusion in quartz from LwsB outcrop1 vein. F) Distribution of FI clusters in jadeite crystals. All these primary inclusions are oriented parallel to c-axis of the clinopyroxene. G) Zoned crystal of omphacite (Omp) from a V2 vein. Note the presence of the FI-rich dark core. H) Biphase and triphase FI in omphacite from V1 vein. The inclusions are oriented parallel to omphacite c-axis and triphase inclusions contain various colorless and opaque solids. I) Triphase 25 μm-long fluid inclusion from a V2 vein. The FI is oriented parallel to omphacite c-axis and contains four colorless solids.

Figure 10: Raman spectroscopy-derived salinity of analyzed fluid inclusions in metasediments and metamafic rocks. A) Measured fluid inclusion salinity for each outcrop, plotted with increasing longitude. Rock units on the Queyras-Monviso transect are characterized by increasing P-T conditions from West (on the left of the graph) to East (right of the graph), thus increasing longitude reflects increasing burial depth. A general salinity-decrease trend with increasing burial depth is observed in metasediments from LPU1 to LPM, while metamafics are generally more saline in both blueschist- and eclogite-facies slices. A 0.4 wt% NaCl eq. uncertainty for salinity values is represented after Caumon et al. (2013). B to E) Cumulative Bar-chart of salinity for each tectonometamorphic unit illustrating the salinity-decrease trend with increasing burial depth in metasediments and the highest salinities in metamafics.

Figure 11: Salinity versus gas content in fluid inclusions from metasediments. Salinity of the liquid phase and amount (mol%) of CO_2 in the CO_2-CH_4 gas mixtures of vapor bubbles were

determined from Raman spectroscopy analyses. LwsB- and Car-bearing veins generally contain more CO_2 than CH_4, while LwsC-bearing vein gas content is dominated by CH_4. A 0.4 wt% NaCl eq. uncertainty for salinity values is represented after Caumon et al. (2013). Simplified graph with all veins in black and white color is on lower right with same units and axes.

Figure 12: Raman spectra of potential hydrocarbons identified in the liquid phase of a FI from quartz of LwsB-bearing vein. CH_2 is identified by its characteristic symmetrical (~2850) and asymmetrical (~2890) stretching vibrations while CH_3 is identified by its characteristic symmetrical (~2920-2930) and asymmetrical (~2960-2970) stretching vibrations. Peak distribution is very consistent with saturated hydrocarbon spectra and especially pentane (Sterin et al., 1980). a.u.: arbitrary unit.

Figure 13: Tentative model of fluid circulation in the Schistes Lustrés complex and geodynamic implications. A) Sketch of W. Alps subduction zone at ~45 Ma. Fluids from blueschist-facies metasediments are low saline with small amounts of CO_2 and CH_4 and expose a decreasing trend of salinity values along depth. In meta gabbros, primary fluids are highly saline and can contain small amounts of N_2 in eclogites. By comparison, unsubducted Helmyntoïdes Flyschs from the alpine accretionary wedge contain low saline fluids with low CH_4 content (Raimbourg et al., 2018). B) Reconstruction of the two possible slicing and stacking sequences of Schistes Lustrés complex units. Its structural upper position in the present day Schistes Lustrés suggests that LPU1 could have been the first detached unit. However, the presence of margin blocks embedded in LPU1 suggest that LPU1 could also correspond to the oceanic units closest to the Piemont margin, thus the latest to be buried and detached from the subducting slab. C) and D) Schematic fluid circulation in LPU1 and LPM at peak burial conditions. FI: fluid inclusions; Sed./Sedim: sediments; Maf.: mafic rocks; Atg-: antigorite-out reaction; Carb.: carbonate-rich layer; Lws: lawsonite; Car: carpholite; Jd: jadeite; Ctd: chloritoide.

Figure 14: Compilation of fluid salinity in primary fluid inclusions from exhumed oceanic subduction rocks. Salinity data series are represented as boxplots and plotted depending on the estimated peak pressure conditions of host rocks. A simplified graph representing mean salinity depending on peak pressure is at the top of the figure. Data series from our study have red names. References for the FI studies and corresponding P-T conditions data are reported in Table 1. Maf.: metamafic rocks; Sed.: metasediments.

Table 1: List of exhumed oceanic subduction zones compiled in figures 1 and 14 and corresponding references for fluid inclusion and P-T estimate studies.

n°	Locality	FI references	P (kbar)	T (°C)	P-T references
1	Helmyntoïdes Flysch, W. Alps	Raimbourg et al. (2018)	?	~270	Raimbourg et al. (2018)
2	Robertson Bay, Antarctica	Rossetti et al. (2006)	2	200-250	Rossetti et al. (2006)
3	Chugach Complex, Alaska	Sisson et al. (1989)	2.5	400-650	Sisson et al. (1989)
4	Kodiak, Alaska	Brantley et al. (1998); Vrolijk (1987); Vrolijk et al. (1988)	2.6 ± 0.4	269	Brantley et al. (1998)
5	Costal Belt, Franciscan Complex, USA	Sadofsky and Bebout (2004)	<3	~125	Blake et al. (1988); Terabayashi and Maruyama (1998)
6	Shimanto Belt, Japan	Raimbourg et al. (2014, 2015, 2018)	3-5	~250	Toriumi and Teruya (1988); Raimbourg et al. (2014)

#	Locality	Reference	P (kbar)	T (°C)	Reference
7	Franciscan Complex - Central Belt, USA	Sadofsky and Bebout (2004)	3-5.6	150-260	Blake et al. (1988); Terabayashi and Maruyama (1998)
8	Otago Schist, New Zealand	Smith and Yardley (1999)	4-5	~390	Yardley (1982); Jamieson and Craw (1987)
9	Southern Appenines, Italy	Invernizzi et al. (2008)	6-8	250-350	Monaco and Tortorici (1995)
10	Franciscan Complex - Eastern Belt	Sadofsky and Bebout (2004)	6-8.3	180-330	Blake et al. (1988); Terabayashi and Maruyama (1998)
11	Franciscan Complex - Diablo Range	Sadofsky and Bebout (2004)	7.4-10.5	130-260	Ernst (1993); Terabayashi and Maruyama (1998)
12	Schistes Lustrés LPU, W. Alps	Agard et al. (2000); Raimbourg et al. (2018)	12-13	300-350	Agard et al. (2001)
13	Rio San Juan Complex, Rep. Dom.	Kawamoto et al. (2018)	12-17	350-500	Shertl et al. (2012); Hertwig et al. (2016)
14	Cerro de Almirez, Betic Cordillera	Scambelluri et al. (2001)	16-19	680-710	Padrón-Navarta et al. (2010)
15	Sapi-Shergol, Himalaya	Sachan et al. (2017)	~19	~17?	Groppo et al. (2016)
16	Tianshan, China	Gao and Klemd (2001)	18-21	480-???	Gao et al. (1999); Gao and Klemd (2000)
17	Tauern Window, E. Alps	Luckscheiter and Morteani (1980); Selverstone et al. (1992)	19.5 ±2.5	590 ± 20	Spear and Franz (1986); Holland (1979)
18	Sanbagawa eclogites, Japan	Yoshida et al. (2015)	20.5	525-565	Endo (2010)
19	Syros, Cyclades	Barr (1990)	22 ± 2	530 ± 30	Laurent et al. (2018)
20	Erro-Tobbio, Ligurian Alps	Scambelluri et al. (1997)	20-25	550-600	Messiga et al. (1995)
21	Samana Peninsula, Rep. Dom.	Giaramita and Sorensen (1994)	22-24	610-625	Escuder-Viruete and Pérez-Estaún (2006)
22	Franciscan Complex eclogites, USA	Giaramita and Sorensen (1994)	22-25	550-620	Tsujimori et al. (2006)
23	Voltri eclogites, Ligurian Alps	Vallis and Scambelluri (1996)	23-25	500-525	Starr et al. (2020)
24 + 24bis	Monviso, W. Alps	Philippot and Selverstone (1991) + Nadeau et al. (1993)	26	550	Angiboust et al. (2011)
25	Rocciavre, W. Alps	Philippot et al. (1998)	25-29	460-610	Ghignone et al. (2020)
26	Lago di Cignana, W. Alps	Frezzotti et al. (2011, 2014); Frezzotti (2019)	>32	590-605	Groppo et al. (2009)

Table 2: Studied samples and corresponding outcrop localities and estimated P-T conditions. P-T conditions estimated from host-rock and segregation parageneses in: [1] Schwartz et al. (2013); [2] Agard et al. (2001); [3] Locatelli et al. (2018). Lws: lawsonite; Qz: quartz; Ank: ankerite; Chl: chlorite; Ph: phengite; Jd: jadeite; Gln: glaucophane; Cal: calcite; Omp: omphacite; Grt: garnet; Ap: apatite; Rt: rutile.

Outcrop	Unit	Peak T / P	Sample #	Host rock	Segregation mineralogy	Longitude	Latitude
1. Château-Queyras	LPU1	332°C[1]/ ~10-13 kbar[2]	1LwsB	Calcschist	Lws-Qz-Ank + late Chl and Ph	6.793083	44.757933
"	"	"	1LwsC	"	"	"	"
2. Guil river	"	328°C[1]/ ~10-13 kbar[2]	2Jd	Metagabbro	Jd-Gln + late Cal	6.817350	44.761550
3. Malafosse	"	336°C[1]/ ~10-13 kbar[2]	3LwsB	Calcschist	Lws-Qz + late Chl and Ph	6.840083	44.771133
"	"	"	3LwsC	"	Lws-Qz-Ank	"	"

Name	Facies	T / P	Sample	Rock type	Assemblage		
"	"	"	3Car	"	Car-Qz + late Chl	"	"
4. Gouret	"	336-367°C[1]/ ~10-13 kbar[2]	4LwsB	"	Lws-Qz-Ank + late Chl and Ph	6.887 066	44.788 583
"	"	"	4LwsC	"	"	"	"
5. Blanche	LP U2	356°C[1]/ ~12-13 kbar[2]	5LwsB	Calcschist	Lws-Qz-Ank-Cal + late Chl and Ph	6.925 016	44.662 983
"	"	"	5LwsC	"	"	"	"
6. Pain de Sucre	"	373°C[1]/ ~13-16 kbar[2]	6LwsB	"	"	6.990 050	44.693 683
"	"	"	6LwsC	"	Lws-Qz-Ank + late Chl, Ph and Cal	"	"
7. Pelvas	LP M	389-402°C[1]/ ~18-20 kbar[2]	7Jd	Metagabbro	Jd-Gln	6.995 666	44.796 806
8. Bric Bouchet	"	402°C[1]/ ~18-20 kbar[2]	8LwsC	Calcschist	Lws-Qz-Ank + late Chl and Ph	7.015 416	44.811 850
9. Valanta	"	469°C[1]/ ~20 kbar[2]	9LwsB	"	Lws-Qz-Ank + late Chl, Ph and Cal	7.063 700	44.683 667
"	"	"	9LwsC	"	Lws-Qz-Ank + late Chl and Ph	"	"
10. ISZ	LP L	580°C/ 27 kbar[3]	10OmpV1a	Metagabbro	Omp-Ap	7.087 500	44.693 889
"	"	"	10OmpV1b	"	"	"	"
"	"	560°C/ 24 kbar[3]	10OmpV2a	"	Omp-Grt	"	"
"	"	"	10OmpV2b	"	"	"	"
"	"	"	10OmpM2	"	"	"	"
11. LSZ	"	580°C/ 27 kbar[3]	10OmpM1	"	Omp-Rt	7.134 166	44.670 000

Declaration of interest statement

The authors declare that they have no known competing financial interests or personal relationships that could have appeared to influence the work reported in this paper.

Highlights:

- Moderately saline aqueous fluids with CO_2 and CH_4 in BS-facies metasediments
- High salinity fluids with solids and N_2 in eclogites fluid inclusions
- Decreasing trend of fluid inclusion salinity along grade in metasediments
- Prograde brine infiltration from continental margin rocks in oceanic metasediments
- High salinity in mafic rocks inherited from seafloor hydrothermal alteration?